National Institute of
Standards and Technology
U.S. Department of Commerce

NIST Technical Note 1553

An Intra-Volume *Ad Hoc* Array Concept for Improved Public-Safety Communications

William F. Young
David W. Matolak
Christopher L. Holloway
Nicolas Bikhazi
Galen Koepke
Helge Fielitz

NIST Technical Note 1553

An Intra-Volume *Ad Hoc* Array Concept for Improved Public-Safety Communications

William F. Young
David W. Matolak
Christopher L. Holloway
Nicolas Bikhazi
Galen Koepke
Helge Fielitz

Electromagnetics Division
National Institute of Standards and Technology
325 Broadway
Boulder, CO 80305

August 2010

U.S. Department of Commerce
Gary Locke, Secretary

National Institute of Standards and Technology
Patrick D. Gallagher, Director

Certain commercial entities, equipment, or materials may be identified in this document in order to describe an experimental procedure or concept adequately. Such identification is not intended to imply recommendation or endorsement by the National Institute of Standards and Technology, nor is it intended to imply that the entities, materials, or equipment are necessarily the best available for the purpose.

National Institute of Standards and Technology Technical Note 1553
Natl. Inst. Stand. Technol. Tech. Note 1553, 60 pages (August 2010)
CODEN: NTNOEF

U.S. Government Printing Office
Washington: 2010

For sale by the Superintendent of Documents, U.S. Government Printing Office
Internet bookstore: gpo.gov Phone: 202-512-1800 Fax: 202-512-2250
Mail: Stop SSOP, Washington, DC 20402-0001

Contents

Executive Summary

This is the seventh in a series of NIST technical notes (TN) on propagation and detection of radio signals in large building structures (apartment complex, hotel, office buildings, sports stadium, shopping mall, etc). The first, second, and third NIST Technical Notes (NIST TN 1540, NIST TN 1541, and NIST TN 1542) in this series described experiments related to radio propagation in a structure before, during, and after implosion. The next two Technical Notes (NIST TN 1545 and NIST TN 1546) focused exclusively on RF propagation into large buildings, with no implosion results. The sixth technical note, TN1552, focused exclusively on the 750 MHz band due to the availability of spectrum between 764 MHz and 776 MHz for a new public-safety band. This technical note departs some from the previous six in this series in that here we present an *ad hoc* array approach for improving radio-frequency coverage in the public-safety environment.

The *ad hoc* array concept was initially introduced in NIST TN 1538 in the form of a boundary condition and optimization analysis problem. The term *ad hoc* array refers to the use of several small communication devices that are randomly placed in an area and hence create a real-time communication network. In large, complex building structures, the signal-to-noise ratio often drops below a sufficient level for establishing a communication link between the transmitter and receiver, thus leaving personnel without radio coverage in sections of the building. This *ad hoc* array concept makes use of the wireless *ad hoc* nodes (a node refers to one communication device) as elements of an array to coherently phase the signals at the receive location (or coherently phase the multiple received signals from a transmitter in the reciprocal process), to increase the signal-to-noise ratio. The single transceiver is typically located in the far-field radiation pattern of the individual array nodes, but within the volume that contains the complete set of *ad hoc* array nodes. Hence, we describe the system as an intra-volume *ad hoc* array.

Simulation results from the initial work and related publications demonstrate the potential benefits of this *ad hoc* array concept. Results provided in this report cover representative real-world measurements of the *ad hoc* array by use of two different measurement techniques. These measurements focus on the frequencies of 750 MHz and 2.4 GHz, and are based on using the array in a receiving and transmitting mode, respectively. The two representative environments were a large basement room with a connected hallway and stairwells, and an atrium between two large office buildings in an urban setting. Key findings are that the *ad hoc* array concept provided gain performance as predicted from previous analysis, simulations, and laboratory experiments. The amount of measured gain ranged from 2 dB to 6 dB for an array of two elements, and up to 10 dB for a four element array. The two element results suggest that using even only two wireless nodes in a coordinated manner can provide significant improvement for public-safety wireless communication systems.

While the primary focus of this effort was to measure the real-world performance of an *ad hoc* array concept, we also provide a different mathematical framework than the original electromagnetic optimization analysis to assist communication engineers in applying the proposed approach to wireless systems in a real-world setting. This combination of measurement results and intuitive mathematical framework serves as the basis from which to design a wireless *ad hoc* array system. The natural next step in the process is to develop wireless nodes and protocols that can implement the *ad hoc* array technique.

An Intra-Volume *Ad Hoc* Array Concept for Improved Public-Safety Communications

William F. Young, David W. Matolak, Christopher L. Holloway, Nicolas Bikhazi, Galen Koepke, Helge Fielitz

Electromagnetics Division
National Institute of Standards and Technology
325 Broadway, Boulder, CO 80305

Here we report on the testing and measurements of an intra-volume ad hoc array concept suitable for public-safety communications in buildings. The term ad hoc array refers to the use of several small communication devices that are randomly placed in an area and hence create a real-time communication network. The overall concept is to use randomly located or placed wireless devices in a coordinated manner in order to increase the radio-frequency signal at otherwise unreachable locations. A typical ad hoc network is limited to a coverage area achieved by the useable coverage of single nodes. We seek to extend the radio-frequency coverage by using two or more nodes (a node refers to one communication device) as elements of an ad hoc phased array. Previous simulations and theoretical analyses have suggested the benefits of the array concept. The measurements presented here, collected in real-world environments, demonstrate that the ad hoc array technique can provide useful gain, up to 10 dB with only four elements. The measurements also indicate a typical gain of 2 dB to 6 dB by use of only two elements.

Key words: ad hoc phased array; emergency responders; multipath; excess path loss; public-safety communications; radio communications; radio propagation experiments; weak-signal detection; wireless array .

1. Introduction

When emergency responders enter large structures (apartment and office buildings, sports stadiums, stores, malls, hotels, convention centers, warehouses, etc.), radio communication to individuals on the outside is often impaired. Mobile-radio and cell-phone signal strength is reduced due to attenuation caused by propagation through the building materials and scattering by the building structural members [1-8]. In addition, a large amount of signal variability may be encountered due to multipath reflections throughout the structures, which can cause severe signal degradation in communication systems.

Here, we report on a project conducted by the National Institute of Standards and Technology (NIST) to investigate the concept of a wireless *ad hoc* array to help mitigate the communications problems faced by public-safety personnel (firefighters, police and emergency medical personnel) in disaster situations involving large building structures. The project was sponsored by the Department of Justice Community Oriented Policing Services (COPS) program through

the NIST Public Safety Communications Research Lab (PSCL). This project focuses on two frequencies, 750 MHz and 2.4 GHz. The 750 MHz band is currently of interest because the FCC is in the process of allocating spectrum between 764 MHz and 776 MHz for a nationwide, next-generation interoperable broadband network for use by the public safety community. The 2.4 GHz band is in a widely used Industrial, Scientific, and Medical (ISM) band.

A possible option to improve radio-frequency coverage inside large buildings is to use *ad hoc* networks that provide node-by-node connectivity (i.e., communication to each node) between the emergency responders and on-site communication facilities. However, these traditional *ad hoc* networks can communicate only within the range of a single node, which means that failure of a single node or insufficient node transmit power, results in a failure of the communication link. This *ad hoc* array actually utilizes several coordinated nodes, thus removing or at least significantly reducing the dependency on any single node. The *ad hoc* array concept could actually be applied to maintain connectivity in a traditional *ad hoc* network if the network experiences segmentation.

An important point about the wireless *ad hoc* array concept tested here is that it is neither a traditional *ad hoc* wireless network nor a traditional phased antenna array. In a traditional wireless *ad hoc* network, the process is to establish node-by-node connectivity. In that case, the transmission range is limited to the range of a single node. A traditional phased-array (when operating in transmit mode) assumes the receiving location is in the far-field of the complete array volume. In our wireless *ad hoc* array, the receiving node is within the volume of the array. Our approach represents a merging of the wireless *ad hoc* network and phased array concepts.

The experiments reported on here took place in two settings, the basement of a two story laboratory/office building and the atrium between two large buildings. Two different systems were used to test the *ad hoc* array concept in receive and transmit modes. A basic description of the wireless *ad hoc* array concept, and a description of the two systems used to test the concept are discussed below.

2. Signal Optimization and Measurement Methods

2.1. Signal Optimization

Use of randomly located wireless devices in an intelligent and coordinated fashion for emergency responders was initially investigated in [9-12]. These initial efforts started with a representation of the optimization problem as infinitesimal dipoles in the presence of several boundary configurations, and used simulation studies to investigate the potential gain available. Optimization means the selection of complex weightings, i.e., phase and amplitude, so that the transmitted signals from the array nodes arrive co-phased at the receive node, with amplitude levels that optimize the aggregate power of the transmitting nodes. In other words, each array node is multiplied by a complex weighting so that the relative amplitudes amongst the nodes are chosen such that those nodes with more power available with respect to the receive location provide the greater contribution. If the environment is free space, then the array nodes closest in Euclidean distance (i.e., direct path) to the receive node provide the most power. However, in a building environment, the closest nodes may not provide the strongest contribution, due to reflections and scattering off furniture, walls, doors, windows, etc. Thus, the complex weights

must account for the effects of the physical environment. References [11], [12] include results from the supporting laboratory experiments that validated the simulation findings. This report covers the next step in the proof-of-concept process, where the testing is extended to real-world settings.

In the optimization, both the power level and the relative phases between the wireless elements are controlled. However, as both the simulation and previous laboratory experiments demonstrate, adjusting of the phase alone accounts for much of the benefit. This simplifies the procedure that devices would need to implement. Thus, here we will use a co-phasing approach, where the individual phases of the *ad hoc* array elements are adjusted so as to add in-phase at the receive location when the array elements are transmitters. (Co-phasing means adjusting the transmitted signal phases of multiple transmit elements such that all the received signals add coherently--see [13], [14].)

The array is either operated in receive or transmit mode. In the receive mode, there is a single transmitter, and the received signals from individual array nodes are co-phased before addition, creating a single received signal. In the transmit mode, each array node is transmitting a signal with additional phase adjustment that ensures co-phasing of all the array elements at a single receive location. In the context of current communication system terminology, the case of a transmit array sending to a single receiver is a multiple-input/single-output (MISO) system, whereas the case of a single transmitter sending to multiple receivers is a single-input/multiple-output (SIMO) system.

The simulation results in our earlier work [9-12] point out some key considerations in constructing a field-deployable implementation. First, diminishing returns in total received power occur once the array contains a small number of transmitters, approximately four transmitters for the optimized case (i.e., both amplitude and phase weighting) and six to eight transmitters for the co-phased case (i.e., only phase weighting). Second, for this same small number of transmitters, the modified directivity results are not significantly different for the optimized and co-phased results [9], [10], [12]. Thus, we propose the following algorithm to obtain the co-phased results, with the recognition that the algorithm also provides a reasonable approximation of the optimized modified directivity. Note that this algorithm pertains to the receive mode operation, and a reciprocal process applies to the transmit mode.

1) Turn on each transmitter individually, and rank the received power of each transmitter.
2) Select the strongest contributing transmitter, and turn it on with all the others off.
3) Select the next strongest transmitter determined in Step 1, and turn it on.
    a. Adjust the phase of this transmitter through 360^0, and determine the phase when the peak power occurs at the receiver. (Note that in these experiments, we are using a mechanical hand-tuned phase shifter. However, previous simulations indicate that stepping at 22.5° will allow the co-phasing process to achieve very near the maximum. We demonstrate this in the receive mode system discussed below by applying a four-bit digital phase shifter to the signals.)
    b. Set the phase of this transmitter to that corresponding to the maximum power at the receiver.

4) Repeat Step 3 for the remaining transmitters (with all previous transmitters on and adjusted), until the desired number of contributing transmitters is reached.

The measurement results here are obtained from the co-phasing approach. An important observation made in [11], [12] is that the co-phasing process is not highly sensitive to the phase deviation. In other words, near maximum gain results are achieved by co-phasing signals within ± 22.5° of each other or a 45° spread.

This process will ensure co-phased transmitted signals at the receiver (for receive mode operations) for however many transmitters are used in the array. If total system or radiated power is not a limitation, all the co-phased transmitters could be included in the process. However, if system power efficiency is important, say for example in a low-power sensor network, then transmit power levels of nodes are weighted such that nodes able to provide more power to the receive location contribute more power, while weaker node contributions are reduced. In free space with omnidirectional radiation, this simply means the power contribution is inversely related to the geometric distance between the array node and the receive location. This combination of selecting power levels and phases is called the complete optimization or the optimized approach, since it optimizes the overall system power; i.e., the aggregate of the array node powers, while ensuring co-phased signals from the array nodes at the receive locations. In an environment such as a building, the optimization process still applies, but the optimal individual power settings are not necessarily inversely related to separation distances.

2.2. Spectrum Analyzer and Mechanical Phase Shifters

2.2.1 Transmitter and Phase Shifters.

The *ad hoc* array was composed of a signal generator that fed radiating antenna elements composing the *ad hoc* array. A 1:8 power divider split the power evenly across the array elements, and mechanical phase shifters allowed adjusting of the phase. The mechanical phase shifters cover 360° at 2.0 GHz, and greater than 360° of phase shift at 2.4 GHz. However, at 750 MHz, the amount of phase shift is less than 150° so this measurement setup was used only for the 2.4 GHz case. Figure 1 shows a diagram of this setup, and Figure 2 displays the various components of the measurement system.

A method of selecting array antenna elements was provided by electro-mechanical relays and selector switches depicted in Figure 2. The output from each phase shifter was either fed into an antenna element via a 36.6 m RF cable or terminated in a 50 Ω load. (The cable loss was approximately 20 dB.) One of the eight output ports from the power divider was terminated in a 50 Ω load connected to a phase shifter for all measurements, because only seven relays were available. Thus, only seven array elements were used in these experiments. Monopoles mounted on aluminum octagon ground planes with an approximate center-to-vertex measurement of 0.24 m were used for the 2.4 GHz antennas. The ground planes were supported by 1.9 cm (¾ inch) diameter polyvinyl chloride (PVC) stands at a height of approximately 1.3 m. Figures 3 and 4 show several of the *ad hoc* array elements at locations in the Building 24 basement and the building in downtown Denver, respectively

2.2.2 Receiving Antenna and Spectrum Analyzer

The performance of the *ad hoc* array was measured by placing a receive antenna either within the volume of the array or in the vicinity of the array boundary. The receiving antenna, identical to the transmitting array element antennas, was connected to a spectrum analyzer via an 18.3 m RF cable, and the measured value was obtained by reading the value displayed on the spectrum analyzer. Depending on how rapidly the channel changed and on the level of the received signal above the noise floor, the waveform displayed on the analyzer exhibited variable rates of fluctuation. However, because the intent of these experiments is not to obtain a precise measurement of the absolute received signal power, but rather to quantify the amount of gain possible by applying the *ad hoc* concept, the precision of visual observation and recording of the power spectrum was deemed adequate. Consistency of results from this manual approach with the automated data capturing system described below demonstrates that the manual measurement approach provides sufficient accuracy.

2.2.3 Multiple Input, Single Output System

The spectrum analyzer and mechanical phase shifters constitute a multiple-input, single-output (MISO) system. We provide a mathematical description of this MISO system, followed by some implementation particulars of the transmitting and receiving components of the system. The mathematical description here differs from the optimization analysis based on approximate boundary conditions used in the earlier works [9-12], and is intended to provide a more intuitive description for communication system engineers. The development here follows from the information theory perspective. A good discussion on MISO, and single-input, multiple-output (SIMO) systems in wireless channels is found in [15].

In the MISO field tests, N transmit antennas were used to send a signal to one receive antenna, ($N = 7$ for the MISO system tests). The source transmit signal was

$$s(t) = A\cos(\omega_c t), \tag{1}$$

where, without loss of generality, we let the phase of the sinusoid be zero. The frequency used was $f_c=\omega_c/2\pi=2.4$ GHz. The input signal has average power $P_s=A^2/(2Z)$ (in watts if A is in volts and the impedance is Z in ohms); as is conventional, for simplicity of signal analysis we let $Z=1\ \Omega$. This signal was split approximately equally in power and connected to the N transmit antennas. Connection was via a power splitter followed by an adjustable phase shifter on each of the N branches. Thus each transmit antenna had an input power of $P_s'/N=\left(A'\right)^2/\left(2Z\right)$ where the primed values of P and A include all losses associated with the power splitter, phase shifters, and the connecting cables. Each transmit antenna experiences nearly equal losses due to the power splitter, phase shifter, and connecting cable. The signal input to the i^{th} antenna can be expressed as

$$s_i(t) = A_i' \cos(\omega_c t + \psi_i + \varphi_i)\ , \tag{2}$$

where $A_i' = A' / \sqrt{2N} = \text{constant}$, and the phases $\{\psi_i\}_{i=1}^N$ are due to splitter, cable, and connector delays, and are nearly identical for all branches. Note that for these tests, the key conditions are that ψ_i is constant and that s_i (amplitude and phase) is approximately equal for all the transmit antennas. The phases $\{\phi_i\}_{i=1}^N$ are the adjustable phases set by the phase shifters, and are used to remove the phase differences due to the propagation paths between transmit and receive antennas in order to achieve the maximum received signal at the receiver (This is evident after convolving with the channel impulse response, as discussed below). Each signal of the form in (2), when output from the antenna, incurs a gain scaling and a phase shift as a function of elevation and azimuth angles. For any given elevation and azimuth angle, we can incorporate the phase shift into the constant phase ψ_i, and can similarly incorporate the gain into A_i'.

Measurements were taken at two different sites, one on the NIST campus in Boulder, CO and the other in downtown Denver, CO. The measurements at the NIST site in Boulder, CO contained a very limited amount of object movement within the array area, i.e., people, and all the receive antenna test locations were indoors. At the Denver site, there was sporadic pedestrian motion in the environment, and vehicular motion outside on the streets. The receive antenna was indoors for all test cases except the first location. Thus, for simplicity we assume the channel is time invariant. For the sinusoidal signals of (2), we can employ the bandpass channel impulse response (CIR), which is given by [16],

$$h_i(\tau) = \sum_{k=1}^{L_i} \alpha_{ki} \delta(\tau - \tau_{ki}) \ , \tag{3}$$

where i indexes the channel from the i^{th} transmit antenna to the receiver, L_i is the number of multipath components in the i^{th} CIR, and the amplitude of the k^{th} multipath component (MPC) in the i^{th} CIR is α_{ki}. The δ is a Dirac delta function, and τ_{ki} represents the delay of the k^{th} MPC of the i^{th} CIR. We can employ values for the MPC amplitudes from measurements, but these will be only approximate. Generally, models consider the α's to be drawn from a random sample with statistics specified by a large number of measurements.

Because the channel is linear, the output of the receive antenna due to the i^{th} transmit signal is given by the convolution of (2) and (3); i.e.

$$\begin{aligned} r_i(t) = s_i(t) * h_i(\tau) &= \sqrt{2P_i} \sum_{k=1}^{L_i} \alpha_{ki} \cos[\omega_c (t - \tau_{ki}) + \psi_i + \phi_i] \\ &= A_i \sum_{k=1}^{L_i} \alpha_{ik} \cos(\omega_c t + \theta_{ki} + \phi_i), \end{aligned} \tag{4}$$

where $\theta_{ki} = \psi_i - \omega_c \tau_k$ can be considered the aggregate channel phase term, which can also incorporate the receive antenna phase. The total signal at the receiver is the sum of the N transmitted signals:

$$r(t) = \sum_{i=1}^{N} r_i(t) = A_i \sum_{i=1}^{N} \sum_{k=1}^{L_i} \alpha_{ik} \cos(\omega_c t + \theta_{ki} + \phi_i). \quad (5)$$

The link distances varied from approximately 3 m to 50 m or more. The channel phase terms are ψ_i-$2\pi \times 2.4 \times 10^9 \tau_{ki}$ for the frequency used for spectrum analyzer system. For these link distances, line-of-sight values of τ_{ki} range from approximately 10 ns to 150 ns, and are even larger for reflected signals. Using this range of values of delay, the channel phase terms span the range of *many* multiples of 2π. Thus representing these phases $\{\theta_{ki}\}$ as random and uniformly distributed on the range [0, 2π), or $0 \le \theta_{ki} < 2\pi$, is a very good model. The phase shifter phases $\{\phi_i\}_{i=1}^{N}$ were adjusted to maximize $|r(t)|$.

While this report focuses on the measured performance of the *ad hoc* array, several simulation results are included to demonstrate the usefulness of analyzing the *ad hoc* array performance with the mathematical framework presented above. The simulation discussion follows the experimental results in Section 4.

2.3. Computer with Channel Sampling Cards

2.3.1 Single Input, Multiple Output System

The first method of data collection constituted a MISO system. However, the reciprocal approach, namely using one transmitter and multiple receiving nodes in an *ad hoc* array manner, i.e., a SIMO system, can also provide similar signal gains. We used a SIMO system discussed below to demonstrate the bi-directional benefit of an *ad hoc* array communication system.

The SIMO system used in the field tests supported automated data capturing with the *ad hoc* array operating in receive mode. In this set of tests, a single transmit antenna was used to send a signal to N receive antennas, where N= 1, 2…6. The transmitted signal is in the same form as (1), but in this case the frequency was f_c=750 MHz. Here we have N individual received signals, each of the form of (4). Each received signal was down-converted and sampled in a separate hardware channel. The individual received signals were then combined at baseband to maximize the amplitude $|r(t)|$ via adjustment of the phases, analogous to the procedure for the MISO tests.

The complex baseband equivalent of (5) is

$$\tilde{r}(t) = A_i \sum_{i=1}^{N} \sum_{k=1}^{L_i} \alpha_{ik}(t) \exp[j(\theta_{ki}(t) + \varphi_i)] \ . \quad (6)$$

The amplitudes and channel phases in (6) are actually slowly-varying functions of time due to the (slowly) time-varying behavior of the channel. Thus, the time dependency is now explicitly shown in the $\alpha_{ik}(t)$ and $\theta_{ki}(t)$ variables.

2.3.2 Transmitter

The fixed transmitter setup included a signal generator outputting a single frequency at 750 MHz, an 18.5 m cable, and a loaded dipole antenna mounted on an aluminum octagon

ground plane with an approximate center-to-vertex measurement of 0.24 m. This same ground plane is used for the 2.4 GHz antennas. The output power on the signal generator was set to 20 dBm, the cable loss was approximately 6 dB, and the gain of the antenna approximately 3 dBi. The antenna and the ground plane were supported by a PVC stand at a height of approximately 1.3 m. Figures 5 and 6 show the 750 MHz setup and data collection system and Figures 7 and 8 show some of the 750 MHz antennas at the Building 24 and Denver experiment sites, respectively.

For one experiment in the Denver building, a handheld 750 MHz transmitter was carried throughout the array volume and perimeter. The transmitter power was set for an output of 30 dBm (instead of the 20 dBm as above), and the "rubber duck" antenna had a gain of approximately 0 dBi (note that this is a different antenna and transmitter from that used for all the other experiments.).

2.3.3 Receiving Antennas and Computer

This automated data capture setup utilized computer cards that sampled six channels directly at 750 MHz, converted the sampled channels to baseband, and then performed the co-phasing algorithm on the six down-converted channels. A raw sample rate of 1 ns was used to capture 8192 instances of the channel samples, for a total capture period of 8.192 μs. These 8192 samples were converted to baseband, and averaged to obtain a single measurement of the received signal, which was then used in the co-phasing algorithm. The overall sampling rate for the processed data was approximately 1.7 samples per second. In this case, a single transmitter provided the signal sampled by the six channels. Each of the six channels was connected via a 36.7 m RF cable to one element of the *ad hoc* array. Each element consisted of an antenna, ground plane, and PVC stand identical to the fixed transmitter setup. An important feature of this automated system is that the channels are sampled simultaneously. Thus, the physical environment is the same for each of six array elements when a particular sample is collected.

This process represents the reciprocal (or "dual") process to use of multiple transmitting elements and a single receive element. In this approach, there are six receive elements and a single transmitter. Changes over time in the physical environment, e.g., pedestrians walking by, and the difference in frequencies i.e., 750 MHz versus 2.4 GHz, mean that the channels may be different. However, the physical locations of the array elements are the same in both cases, and the same co-phasing algorithm is applied to the received signals. Due to frequency limitations of the cards, this process was performed only at 750 MHz. The specific cards used in the experiments are the CompuScope 21G8, and the data sheets are available at [17]. The computer was a Dell Precision 380 running Windows XP, with a Pentium D 3.0 GHz processor and 2 GB of memory. Mention of any company names serves only for identification, and neither constitutes nor implies endorsement of such a company or of its product by NIST.

3. Building Structure Descriptions and Experimental Set-up

This section briefly describes the two building structures used in these experiments, and the experimental setup. While the locations of the *ad hoc* array were essentially random, the general locations of elements were chosen to test possible field-deployment configurations. For example, two of the array elements were placed in a hallway off the main room in the NIST Building 24

experiments, while three array elements were placed outside of the atrium at the Denver experiment. Both cases represent possible deployment configurations of an *ad hoc* array system by emergency responders. More specifics on the two experimental sites follow below.

3.1 NIST Building 24, Boulder, Colorado

Building 24 on the NIST, Boulder campus is a combination laboratory and office structure. The structure is composed of typical building materials, including concrete, steel, drywall, and acoustic ceiling tiles. The section used for the array tests consisted of a large, open room in the basement, a connected hallway on the same level, landings in two stairwells that connected the basement to the upper floors, and a small bathroom at the basement level. Figure 9 shows the layout of the *ad hoc* array elements and the test locations. Test locations represent either a receive antenna connected to the spectrum analyzer for the 2.4 GHz measurements or a transmit antenna connected to the signal generator for the 750 MHz measurements. Note that array element E is not used in the sampling cards and computer data collection, as the system has only six available channels.

Three important features of the array layout and test locations are: (1) the placement of two array elements in the hallway, which represents the case when array nodes are located in the hallway of a building, (2) the inclusion of a test location within a bathroom, which represents the case when an array node is located in a separate room, and (3) the location of an array element and test location on stairwell landings approximately 1.3 m above the basement floor level, which represents the case when the array and single receiving/transmitting node are located at different elevations in the building. Figure 3 and Figure 7 show some of the basement features, including the concrete block walls and the unfinished ceiling.

3.2 555 17th Street, Denver, Colorado

The 555 17th Street location is an atrium or enclosed lobby area between two buildings in downtown Denver. (We refer to the location as the Denver site.) The structural construction materials are a typical high-rise combination of concrete, glass, and steel, and the lobby area consist primarily of stone, glass, and metal frames. The layout of the *ad hoc* array elements and the test locations both within the atrium and on the sidewalk adjacent to the building are shown in Figure 10.

Two key features of this layout are: (1) the placement of the three array elements, A, B, and C, on the sidewalk outside of the atrium area, and (2) the location of test point 1 outside the main entrance of the atrium. This is to emulate the use of the array concept to help with signal penetration into the building. The experiments in Denver also include a scenario in the 750 MHz test where a handheld transmitter is carried on an arbitrary path along the sidewalk where A, B, and C are located, and throughout the atrium.

4. Experimental Results

The experimental results for Building 24 and the Denver site are provided for both measurement systems in the layouts and test locations described previously. As is evident in the data plots, the

computer system with the network cards allows the collection of a much greater amount of data over a given period. However, overall results show consistent behavior between the two approaches, and both validate the *ad hoc* array concept.

The expected combined systematic and random errors introduced by our measurement equipment are expected to be on the order of tenths of decibels. Two different data collection methods were used for the two different frequencies. For the 750 MHz test, an automated system was used, and either 50 or 100 samples were collected at each test position. The repeatability for these 50 to 100 samples were within 0.5 dB. This variability is due mainly to the propagation channel changing during the experiments caused by objects moving during the experiments. While no repeatability data were obtained for the 2.4 GHz measurement, the uncertainties in both this set of experiment are believed to be less than 1dB.

4.1 Spectrum Analyzer Measurement Results

Figures 11 to 16 show the application of the co-phasing algorithm to the 2.4 GHz case, or the transmit mode. The first set of figures, Figures 11 and 12, show the raw results of the co-phasing process. In the Building 24 case, from one to seven transmitting elements were used for all eight of the receiving or test locations. At the Denver site, from one to seven transmitting elements were used for five of the test locations, and from one to six transmitting elements were used for the remaining two test locations (test locations 3 and 7). In the case of test location 3, array element G was not included, due to the close proximity to avoid dominating overall performance by a single element (G). At test location 7, array element D was not included for the same reason. Both of these cases represent conditions where the array concept would be unnecessary since there is a very strong signal emanating from the nearby node.

While the increase in recorded power provided by adding co-phased elements is evident in the raw data, due to the difference in distances from array elements at various test locations, the relative increase is not obvious. Figures 13 and 14 display the relative increase by normalizing the data with respect to the strongest contributing element. Thus, the initial single element starts at 0 dB for all test positions. The results for Building 24 in Figure 13 indicate an increase of 1 dB to 6 dB when the second array element is included. The 6 dB increase is at the theoretical upper bound, assuming identical gain patterns from the antennas at the test location. In other words, assuming that each array element is capable of establishing the same electric field level at the test location, with two elements, at best, the electric field magnitude can be doubled. This corresponds to a 6 dB increase in power.

For the Denver site results shown in Figure 14 for test locations 4 and 6, the gain from two elements is 6.3 dB and 6.1 dB, respectively. This would appear to be a violation of the theoretical maximum; however, that maximum does not take the environment into account. In the case of test location 4, there is a column near the receiving antenna, which affects the antenna gain pattern. Similarly, many of the array elements are near objects that affect the antenna gain patterns. Thus, we do not expect identical performance from each array element. In addition, if the test location resides in a deep null, then any slight change in the physical environment (i.e., pedestrian movement, door opening, etc.), can significantly change the measured power.

One of the important factors for a practical system is determining the number of array elements to utilize. Figure 13 indicates that the gain increase from one to four elements ranges between 2 dB to 10 dB. However, the increase from four to seven elements only provides an increase of approximately 1 dB (which is approaching the measurement uncertainty). In Figure 14, the gain increase from one to four elements ranges between 5.5 and 10 dB. Similar to the results in Figure 13, the increase of four to six or seven elements provides only about a 1 dB increase. Thus, while the Building 24 case shows a wider range of gain at four array elements, both the Building 24 and the Denver site results show very similar behaviors on the upper limit of four elements and in the trend from four to seven elements (Note that the theoretical upper limit for normalized power in free space is an N^2 curve. Thus, for four elements the maximum theoretical power gain would be 12 dB, and 16.9 dB for seven elements, assuming a free-space environment and equal contribution from the elements at the test location).

A key aspect of a practical system is the ability to increase a weak signal to a level that supports communication. Clearly, if the signal is sufficiently strong already there is minimal value to the *ad hoc* concept. However, the array concept can help raise a weak signal to a useable level. Another important aspect of the array concept is the ability to extend the perimeter or boundary of communication connectivity. Figure 15 and Figure 16 demonstrate that two elements can be used to (1) raise the signal to a useable level, and (2) extend the communications boundary.

In Figure 15, the two elements located in the hallway off the main room in the basement are co-phased to extend the communication boundary. If one of the signals is well above the noise floor, the addition of another weak signal provides little benefit; e.g., see receive test position 3 in Figure 15. However, receive test positions 7 and 8 both demonstrate how using two elements can provide substantial gain in the signal. As discussed above, there initially appears to be a violation of the 6 dB maximum possible at receive position 8. This is likely due to not starting from the absolute maximum for each individual element; i.e., not adjusting the phase to account for the multipath created by a single element. It is interesting to note that, other than receive test locations 3 and 6, all receive test locations indicate a gain of at least 2 dB by use of these two elements in the hallway.

Figure 16 shows the results for two array elements at the Denver site. In this case, receive test position 4 provides a gain of almost 15 dB. This better than expected maximum behavior is likely due to not establishing the individual maximum for each of the two elements before optimizing the combination of the two. In other words, the two elements may each have been creating a deep self-null due to several multipath contributions, while the co-phasing process in the phase adjustment removes the self-null and maximizes the contribution of the second element. However, more importantly, across all receive positions, at least 1 dB of gain was realized, and in most cases, more than 2 dB was possible when two relatively weak signals were co-phased.

4.2 Channel Sampling Card Measurement Results

The data collection and subsequent application of the co-phasing algorithm to the 750 MHz signals provides results consistent with the data at 2.4 GHz discussed above. Recall that the

channel was initially sampled at a much higher rate, down-converted to baseband, averaged to obtain an estimated representation of the signals received by each antenna, and then processed according to the co-phasing algorithm. All the results presented here are from the processed data.

Figures 17 to 32 show the results from applying the co-phasing algorithm with the transmitter located at the eight different test points in Building 24. Figures 17, 19, 21, 23, 25, 27, and 31and are the total power results versus the sample number. These results illustrate how the inclusion of more array elements increases the total power. The 50 samples represent a total measurement period of approximately 86 seconds.

The corresponding order in which array elements are added to the cumulative sum is depicted in Figures 18, 20, 22, 24, 26, 28, 30, and 32. The RX antenna positions refer to a particular array element as the *ad hoc* array is receiving in this case. The order number refers to the order in the cumulative sum; that is, 1^{st} means the first element in the sum, 2^{nd} mean the second element in the sum, etc. The elements are added into the cumulative sum from strongest to weakest contributions, so the 1^{st} element is the strongest contributor, the 2^{nd} element is the next strongest contributor, and so on. Most of the test positions, which in this system represent transmitter locations, exhibit little change in the ordering for the cumulative sum. Two factors that will affect the order are people or objects moving through the array and comparable signal strengths of the elements. In the Building 24 measurements, the change of ordering can largely be attributed to the comparable signal strengths since there were no moving objects or people within the array. For example, Figure 32 indicates some reordering between the 2^{nd}, 3^{rd}, and 4^{th} array elements, but the 1^{st}, 5^{th}, and 6^{th} elements remain the same for all 50 samples. This indicates that the signal levels of the 2^{nd}, 3^{rd}, and 4^{th} elements are nearly equal, and thus any slight change in the measured signal will cause the order of contribution to the cumulative sum amongst these three elements to change. The 1^{st}, 5^{th}, and 6^{th} elements signals are sufficiently distinct that their order of contribution does not change.

Figures 33 to 46 show the results for the seven fixed transmitter locations at the Denver site. Figures 33, 35, 37, 39, 41, 44, and 45 and are the total power results versus the sample number. At the Denver site, 100 samples were collected over a period of approximately 173 seconds. Note that at the Denver site, some collection positions include samples at the start when the transmitter is not on. Figures 34, 36, 38, 40, 42, 43, and 46 indicate the order of the array elements in the cumulative summation process. In general, a little more reordering appears as compared to the Building 24 case, but for each of the seven transmitter locations, the initially selected receive element remains the same each sampling (ignoring the first few samples when the transmitter is turned off). People were moving through the array area at the Denver site, and this is the probable cause of changes in the element summation order.

At the Denver site, one experiment consisted of walking a handheld transmitter around the *ad hoc* array area to capture some of the dynamic nature of the *ad hoc* array. Figures 47 and 48 show the co-phased cumulative sum and the order of the contributing receive elements, respectively. 150 samples were collected over a period of approximately 255 seconds. In this case, the transmitter power was set to 30 dBm. Figure 47 exhibits greater than a 40 dB range. The lowest total power, near sample 50, occurs when the transmitter was carried along the

sidewalk, well away from any of the array elements. Figure 48 shows significant changes in the array element order, which is expected, because the transmitter location is changing.

4.3 Alternate Representation of Sampling Card Results

Averaging of several samples from the previous results for the sampling cards allows a more direct comparison to the spectrum analyzer measurements. In Figures 49 and 50, the raw power is plotted versus of the number of array receiving elements for Building 24 and the Denver site, respectively. These values are computed by averaging the results from sample number 5 to 45 for the Building 24 data, and sample numbers 15 to 85 for the Denver site (these data ranges where chosen to avoid including any data collected during the off/on and on/off transitions of the transmitter). The total power is generally greater than the spectrum analyzer data because of the in-line amplifiers used with the sampling cards. (There are other loss factors not included with the sampling card system, such as the power divider loss.)

For comparison purposes, the normalized cumulative power is plotted in Figures 51 and 52 for Building 24 and the Denver site, respectively. Figures 51 and 52 compare to Figures 13 and 14, respectively, though a true direct comparison is not possible, because the spectrum analyzer results are for 2.4 GHz and the sampling card results are for 750 MHz. However, similar to the spectrum analyzer results, for most of the test positions, the gain is between 2 to 6 dB when the second element is included and the rate of gain increase beyond four elements drops significantly. Test position 3 for the Denver site shows less than 2 dB of gain even at six array elements because of the close proximity of the transmitter and the receiving array element located at G. (Recall that this array element was not included in the spectrum analyzer data for test position 3.) Test position 7 in Building 24 behaves nearly the same for both measurement systems, which is likely due to the fact that the test position is elevated above the array plane.

4.4 Log-distance Path Loss Exponent Estimation by use of the *Ad hoc* Array

The data collected to demonstrate the array concept can also provide insight into the propagation environment in the presence of the array. This analysis examines the path loss characteristics of the environment, and in particular, estimates of the path loss exponent are provided. Reference [16] contains relevant material on path loss calculations and typical results.

The following equation is used to estimate the path loss exponent, n,

$$\begin{aligned} P(d_i)\,\text{dBm} &= P_0\,\text{dBm} - PL(dB) \\ &= P_0\,\text{dBm} - 10n\log(d_i / d_0), \end{aligned} \tag{7}$$

where i is the array element at a distance d_i from the test location, d_0 is the distance between the array element used as the reference and the test location, and P_0 is the measured power of the reference array element. Since only one measurement was taken at each location, the typical additional random variable is not included on the right side of (7), for example, see equation (4.93) in [16]. Also, the path loss for the location d_0 is accounted for in the measured power at that location, and that d_0 is the location with the strongest contributing array element to the

among all possible test location. Thus, for the 2.4 GHz case in Building 24, the d_0 is the distance between array element E and test location 5; for the 2.4 GHz in Denver, d_0 is the distance between array element D and test location 7; and for the 750 MHz case in Denver, d_0 is the distance between array element G and test location 3. Note that a path loss exponent of $n = 2$ is assumed for the reference location, which corresponds to free space. The 750 MHz case for Building 24 was not included, because a clear reference pair could not be established. This is because the array element location E was not included in the 750 MHz data collection, and all other possible combinations included objects or orientations in the path between the transmitter and receiving element, so that there was no reasonable choice for P_0 and the associated d_0. Note that in order for (7) to be a valid estimate, $d_i > d_0$ and $P(d_i) < P_0$ are required.

Figures 53 and 54 show the 2.4 GHz case for Building 24 and the Denver site, respectively. The n values range from 1.1 to 5.7, which is consistent with results presented in [16]. Note that an n value of less than 2 implies a waveguide affect. Further examination of Figure 53 reveals an average of $n = 3.6$ for test location 7, which is due to the fact that the test location is not at the same elevation as the array elements. The average of $n = 3.1$ at test location 8 is due to the additional walls and obstructions between the array elements and the receive test antenna as compared to test locations 1 to 6.

Figure 54 indicates an average path loss exponent of between 1.9 and 2.4 at 2.4 GHz, which more closely tracks the behavior of free space ($n = 2$) than the results from Building 24. This is expected, because the atrium area is a more open environment than the basement in Building 24. The path loss exponent for the Denver building ranges from 1.1 to 3.2, as compared to a range of 1.3 to 5.7 for Building 24.

The 750 MHz path loss exponent estimations are shown in Figure 55. The average of 2.0 to 2.6 indicates a behavior slightly worse than that of free space, but is consistent with the results for 2.4 GHz. Useful 750 MHz results were not available for Building 24, due to the lack of a good reference position within the array topology relative to the test locations. The reference location used for the 2.4 GHz case in Building 24 was not included in the 750 MHz measurements.

5. Measured Data versus Simulations

We tested the analytic expression in (5) against our measured data subject to several approximations discussed below. As illustrated below, the simulations compare favorably with the measured results. We compare the normalized results from the simulations and measured data, because this removes the need to accurately predict absolute power levels, and because the *ad hoc* array gain rather than the absolute power level is our quantity of interest. Thus the following assumptions and parameter values are used:

1) $A = 1$
2) t = constant
3) $\omega_c = 2\pi \times$ frequency
4) θ_{ki} = uniformly random over $[0, 2\pi)$
5) φ_{im} = adjusted to maximize $r(t)$, in m discrete steps over $[0, 2\pi)$; $m = 16$ for these simulations

6) $N = 6$ or 7, the number of *ad hoc* array elements
7) $L_i \geq 1$, (one corresponds to no multipath contribution)
8) $\alpha_{i1} = 1/d_i$, where d_i is the distance between the i^{th} array element and the test location
9) $\alpha_{ik} = (1/d_k)^{n/2}$, where d_k is uniformly random over [5, maximum of $2 \times d_i$], and n is uniformly random over [2.5; 6].

In these MISO simulations, the test and array element locations are those used in the actual measurements, listed in Figures 9 and 10. These distances are the dominant factors in the simulated array performance. The α_{ik} values provide a very rough approximation of the multipath contribution; more precise values can likely be extracted from other measured data. A simulation run averaged 10,000 trials, where a trial consisted of selecting a random value for θ_{ki}, and α_{ik} over the intervals specified above, and then performing the co-phasing algorithm in the simulation. Setting the time variable of t as a constant means that the simulation results correspond to a specific instant in time. Thus, the $\omega_c t$ variable becomes a constant phase offset. A more exact simulation would incorporate both the time and frequency dependence of α_{ik}, although as previously noted, the channel can be considered time-invariant for a large fraction of the time. Note that the results from the channel sampling measurement system indicated that channel was generally not changing rapidly with respect to time, at least not enough to change the order of the array elements in the co-phasing algorithm.

Simulation results based on the *ad hoc* array and test locations are shown in Figures 56 to 59. Figures 56 and 57 are based on the Building 24 locations, while Figures 58 and 59 are based on the Denver site. In Figures 56 and 58, no multipath contribution is included, which represents a "free space" environment. Figures 57 and 59 include ten multipath components in addition to the direct path. The most noticeable difference between the free space and multipath simulations is the spread of values for a given number of elements (2 or more). For example, the two element case for Building 24 has a spread of approximately 4 dB for free space and a spread of approximately 2 dB for the multipath case. Excluding test location 3, the Denver site exhibits a similar decrease as multipath components are included. Both Building 24 and the Denver site show a decrease in the maximum for test location 4 (using six array elements) of approximately 1 dB in the multipath versus free space.

The simulation results correspond to the normalized *ad hoc* array measurements. For Building 24, Figures 13, and 51, compare to Figures 56 and 57, and for the Denver site, Figures 14 and 52 compare to Figures 58 and 59. In the Building 24 case, simulation results do not predict as wide a spread of values, which is likely due to the lack of incorporating impacts of local obstacles on the antenna gain pattern, and to inaccuracies in multipath amplitude and phase modeling. Weighting due primarily to the distance would be more accurate when the antennas radiate in a true omnidirectional pattern associated with a point source. The rate of gain increase is similar between the simulations and the measured data up to inclusion of the first four elements. However, the measured results appear to reach a diminishing return point near the four-element mark. This is due in part to the additional signals being near or below the noise floor of the measuring equipment, which is not accounted for in the simulation.

Simulations and measurements of the Denver site compare reasonably well, particularly when the measurements are taken from the sampling card results (Figure 52). Note that the spectrum

analyzer measured results in Figure 14 do not include array element G for the case of test location 3, which dominates the other array elements in the simulations and the sampling card measurements. As pointed out in the path loss exponent estimation above, the Denver site behaves much like a free-space environment, so the closeness of match with the simulations is expected.

6. Summary of Results and Conclusion

The primary focus of this effort was to measure the performance of an intra-volume *ad hoc* array concept to improve public-safety communications. We also provided a mathematical framework, different from the original optimization analysis, to assist communication engineers in applying the proposed approach to wireless systems in a real-world setting. Simulations based on the descriptive mathematics and some rough approximations indicate a reasonable prediction of the *ad hoc* array behavior. The combination of the measurement results and the mathematical framework serves as the basis from which to design a wireless *ad hoc* array system for public safety.

Two different measurement systems tested the intra-volume *ad hoc* array concept in a transmit mode (MISO), using mechanical phase shifters at 2.4 GHz, and in a receive mode (SIMO) with channel sampling cards at 750 MHz. Measurements were carried out at two different building sites, one in a large basement and the other in an atrium between two large office buildings. Subject to differences in frequency dependencies of materials and the surrounding environment, the array concept performed equivalently in transmit and receive modes, as expected.

Major measurement findings are: (1) the *ad hoc* array concept does provide gain performance consistent with earlier predictions; (2) the gain typically ranged from 2 dB to 6 dB for two array elements, and up to about 10 dB for four array elements; (3) the gain per element starts to reach diminishing returns at around four elements, and (4) the coordinated use of only two elements can provide a significant gain improvement. The fourth point is important, because two wireless nodes are generally easier to coordinate than three or more, and suggests that meaningful improvement in public-safety communications can be achieved by use of two wireless nodes as a two-element array.

Further refinement of analysis in the presence of multipath propagation, and extension to modeling of modulated signals are two areas of future work. The natural next step in the process is to develop wireless nodes that can implement the *ad hoc* array technique.

Disclaimer: Mention of any company names serves only for identification, and neither constitutes nor implies endorsement of such a company or of its products by NIST.

This work was sponsored by the U.S. Department of Justice through the Public Safety Communications Research Lab, Derek Orr, Program Manager. We thank members of the

technical staff of the Electromagnetics Division 818, who assembled the test equipment, and Michael Francis and Perry Wilson for managerial support. We also thank Patrick Fine and his staff for providing access to the 555 17th Building in Denver, Colorado

7. References

[1] Statement of Requirements: Background on Public Safety Wireless Communications, The SAFECOM Program, Department of Homeland Security, Vol. 1, March 10, 2004.

[2] M. Worrell and A. MacFarlane, Phoenix Fire Department Radio System Safety Project, Phoenix Fire Dept. Final Report, Oct. 8, 2004, http://www.ci.phoenix.az.us/FIRE/radioreport.pdf

[3] 9/11 Commission Report, National Commission on Terrorist Attacks Upon the United States, 2004.

[4] Final Report for September 11, 2001 New York World Trade Center terrorist attack, Wireless Emergency Response Team (WERT), Oct. 2001.

[5] C.L. Holloway, G. Koepke, D. Camell, K.A. Remley, D.F. Williams, S. Schima, S. Canales, and D.T. Tamura, "Propagation and Detection of Radio Signals Before, During and After the Implosion of a Thirteen Story Apartment Building," NIST Technical Note 1540, Boulder, CO, May 2005.

[6] C.L. Holloway, G. Koepke, D. Camell, K.A. Remley, and D.F. Williams, "Radio Propagation Measurements During a Building Collapse: Applications for First Responders," Proc. Intl. Symp. Advanced Radio Tech., Boulder, CO, March 2005, pp. 61-63.

[7] C.L. Holloway, G. Koepke, D. Camell, K.A. Remley, D.F. Williams, S. Schima, and D.T. Tamura, "Propagation and Detection of Radio Signals Before, During and After the Implosion of a Large Sports Stadium (Veterans' Stadium in Philadelphia)," NIST Technical Note 1541, Boulder, CO, October 2005.

[8] K. A. Remley, G. Koepke, C.L. Holloway, C, Grosvenor, D. Camell, J. Ladbury, J. T. Johnk, D. Novotny, W. F. Young, G Hough, M. C. McKinley Y. Becquet, J Korsnes, "Measurements to Support Broadband Modulated-Signal Radio Transmissions for the Public-Safety Sector, " NIST Technical Note 1546, Boulder CO, April 2008.

[9] W. F. Young, E. F. Kuester, C.L. Holloway, "Optimized Arbitrary Wireless Device Arrays for Emergency Response Communications," NIST Technical Note 1538, Boulder CO, March 2005.

[10] W. F. Young, E. F. Kuester, C. L. Holloway, "Optimizing Arrays of Randomly Placed Wireless Transmitters for Receivers Located Within the Array Volume," Antennas and Propagation, IEEE Transactions on, vol.55, no.3, pp.698-706, March 2007.

[11] W. F. Young, E. F. Kuester, C. L. Holloway, "Measurements of Randomly Placed Wireless Transmitters used as an Array for Receivers Located within the Array Volume with Application to Emergency Responders," Antennas and Propagation, IEEE Transactions on, vol.57, no.1, pp.241-247, March 2009.

[12] W. F. Young, "Optimizing Arrays of Randomly Placed Wireless Transmitters with Receivers Located in the Array Volume," Dissertation, University of Colorado at Boulder, 2006.

[13] M. I. Skolnik and D. D. King, "Self-phasing array antennas," IEEE Trans. Antennas Propag., vol. 12, no. 2, pp. 142–149, Mar. 1964.

[14] L. D. DiDomenico and G. M. Rebeiz, "Digital communications using self-phased arrays," IEEE Trans. Microw. Theory Tech., vol. 49, no. 4, pp. 677–684, Apr. 2004.

[15] G. D. Durgin, "Space-Time Wireless Channels," Pearson Education, Inc., Publishing as Prentice Hall, Inc, Upper Saddle River, NJ, USA, © 2003.

[16] T. S. Rappaport, "Wireless Communications: Principles and Practice, 2nd Edition," Chapter 4, Prentice Hall, Inc, Upper Saddle River, NJ, USA, © 2002.

[17] Cobra CompuScope 21G8, GaGe Cobra™, http://www.wuntronic.eu/index.php?site=2&xid=65&subid=185&sub2id=186&pid=255

Appendix I: Experiment Setups and Locations

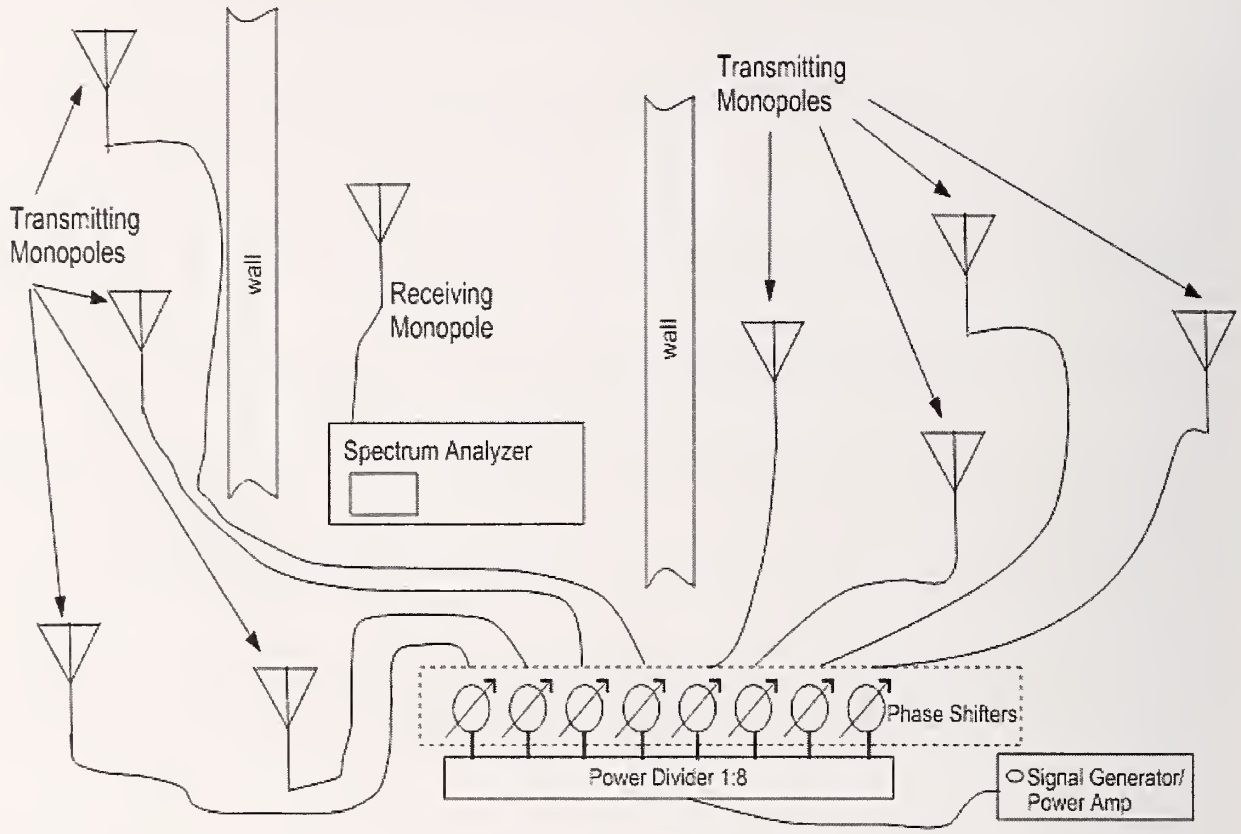

Figure 1. Sketch of experimental setup where a signal generator, power divider, and series of mechanical phase shifters provide power to transmitting monopoles mounted on individual ground planes. The receiver setup consists of a monopole on a ground plane connect to a spectrum analyzer. 120 foot (≈37 m) cables connect the transmitting monopoles to the phase shifters. A 60 foot (≈ 18 m) cable connects the receiving monopole to the spectrum analyzer. This is the setup used for the 2.4 GHz measurements.

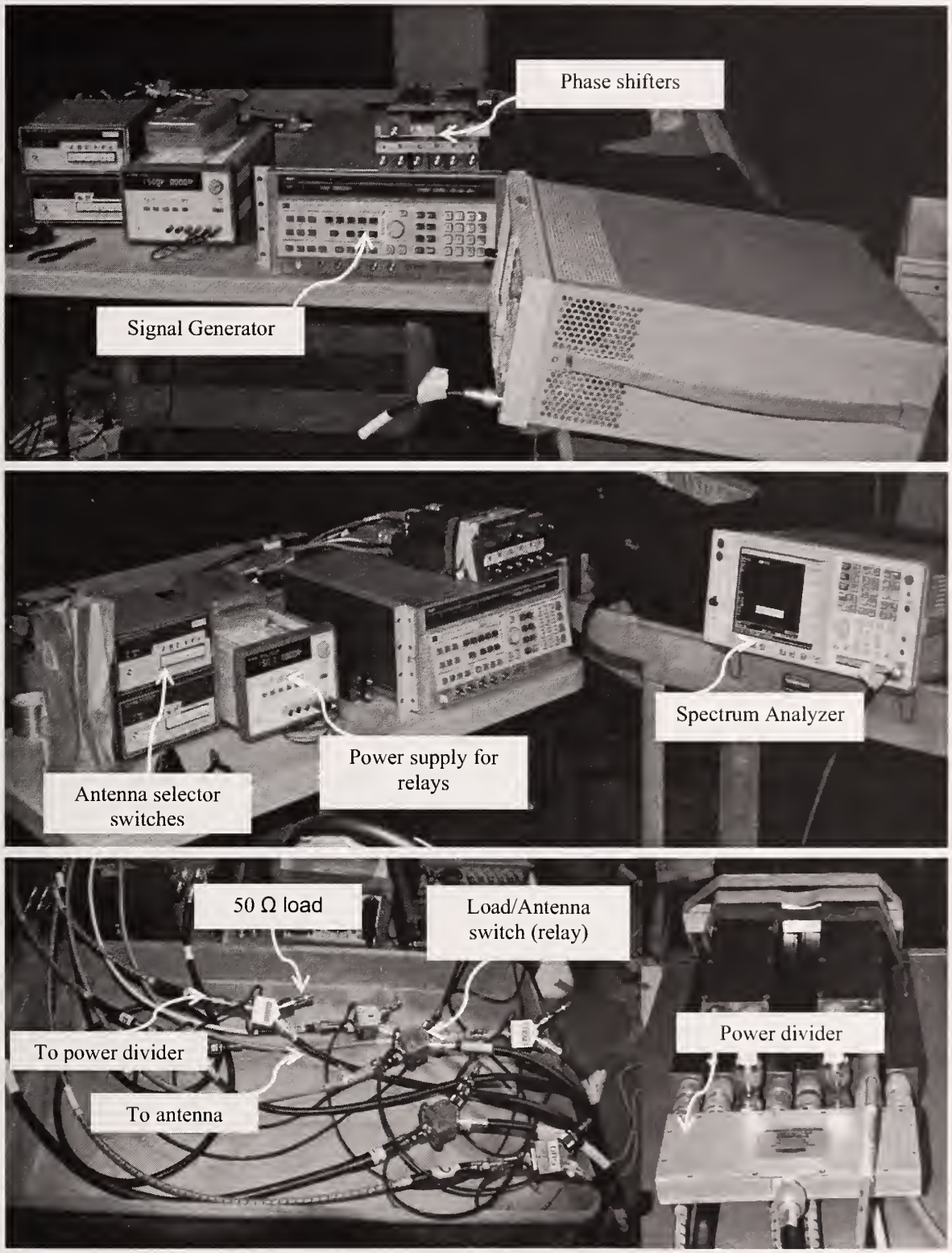

Figure 2. Pictures of equipment used for the 2.4 GHz experiments. Power is supplied to seven monopole antennas through a single signal generator and a power divider. The output of the power divider is either fed to an antenna or terminated in a 50 Ω load. The spectrum analyzer measures the received power at the single receive antenna, and the phase shifters are used to adjust the relative phase between transmitting antennas.

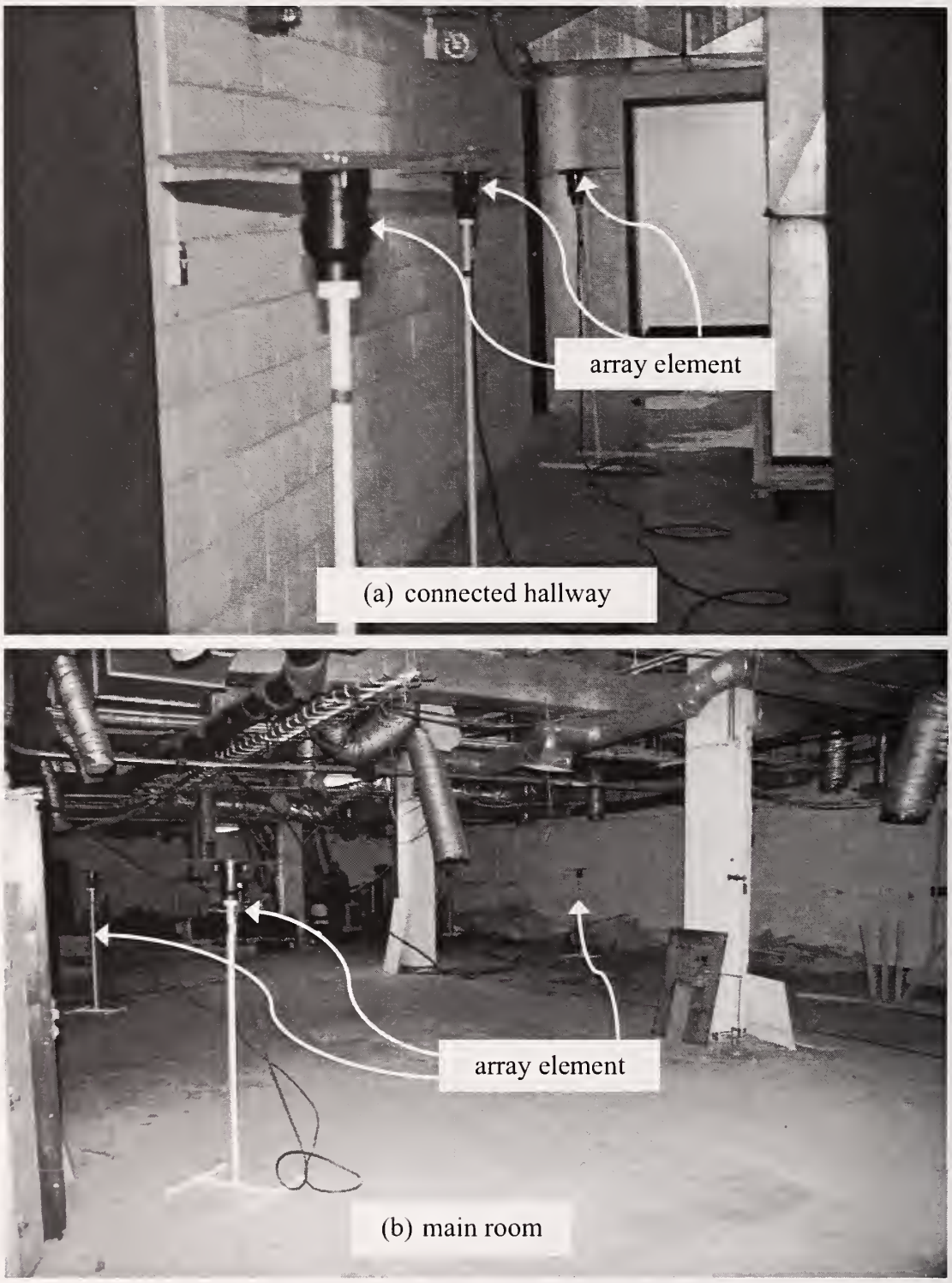

Figure 3. Several of the 2.4 GHz antennas used in the 2.4 GHz experiments in the basement of Building 24, both in the main room and the connected hallway.

Figure 4. Some of the 2.4 GHz antennas used in the 2.4 GHz experiments at the Denver location, both inside and outside of the atrium area.

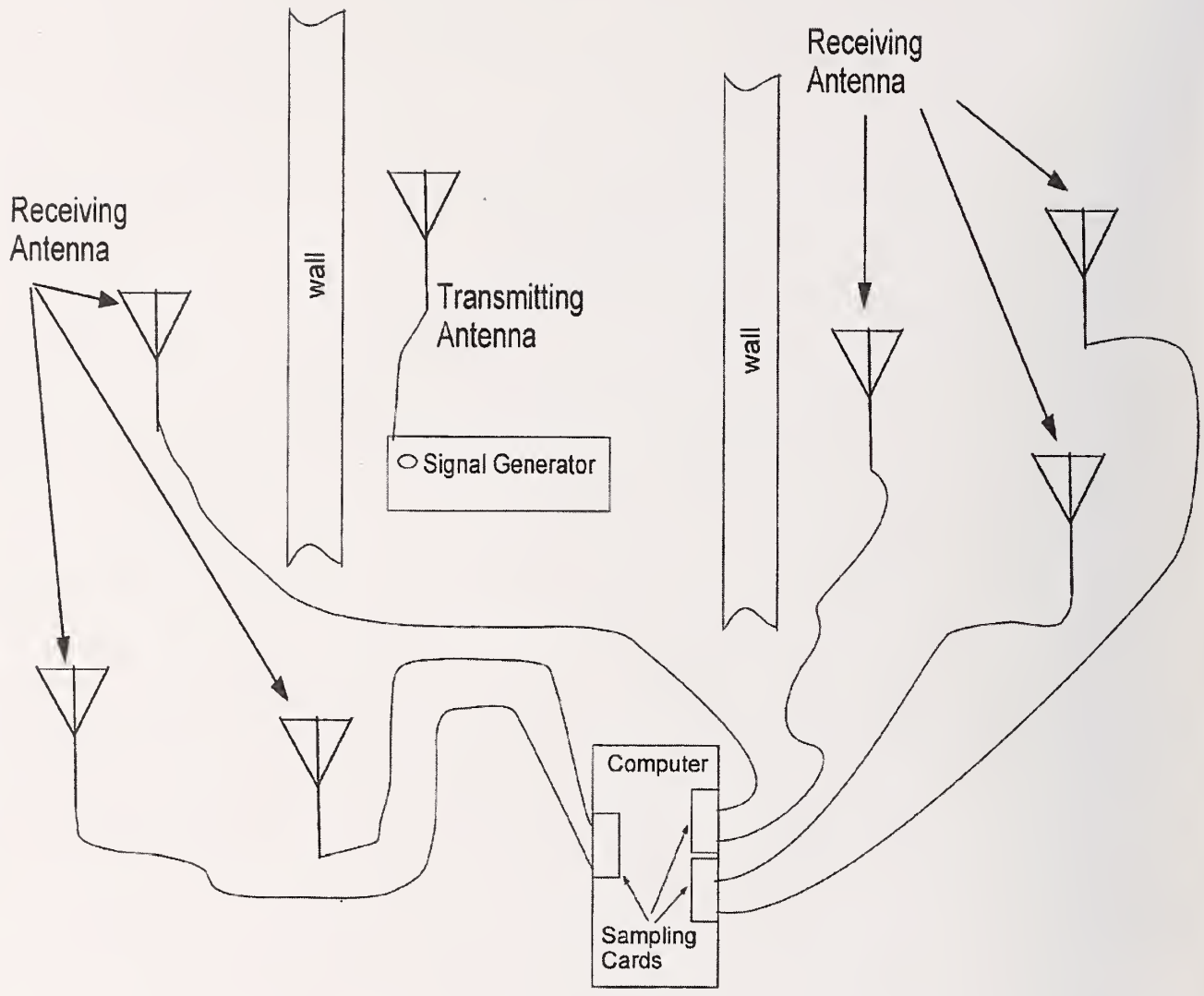

Figure 5. Sketch of experimental setup where a signal generator and mechanical phase shifters provide power to the transmitting antenna mounted on a ground plane. The receiver setup consists of six antennas on individual ground planes connected to computer with RF sampling cards. 120 foot (≈37 m) cables connect the transmitting monopoles to the phase shifters. A 60 foot (≈ 18 m) cable connects the receiving monopole to the spectrum analyzer. This is the setup used for the 750 MHz measurements.

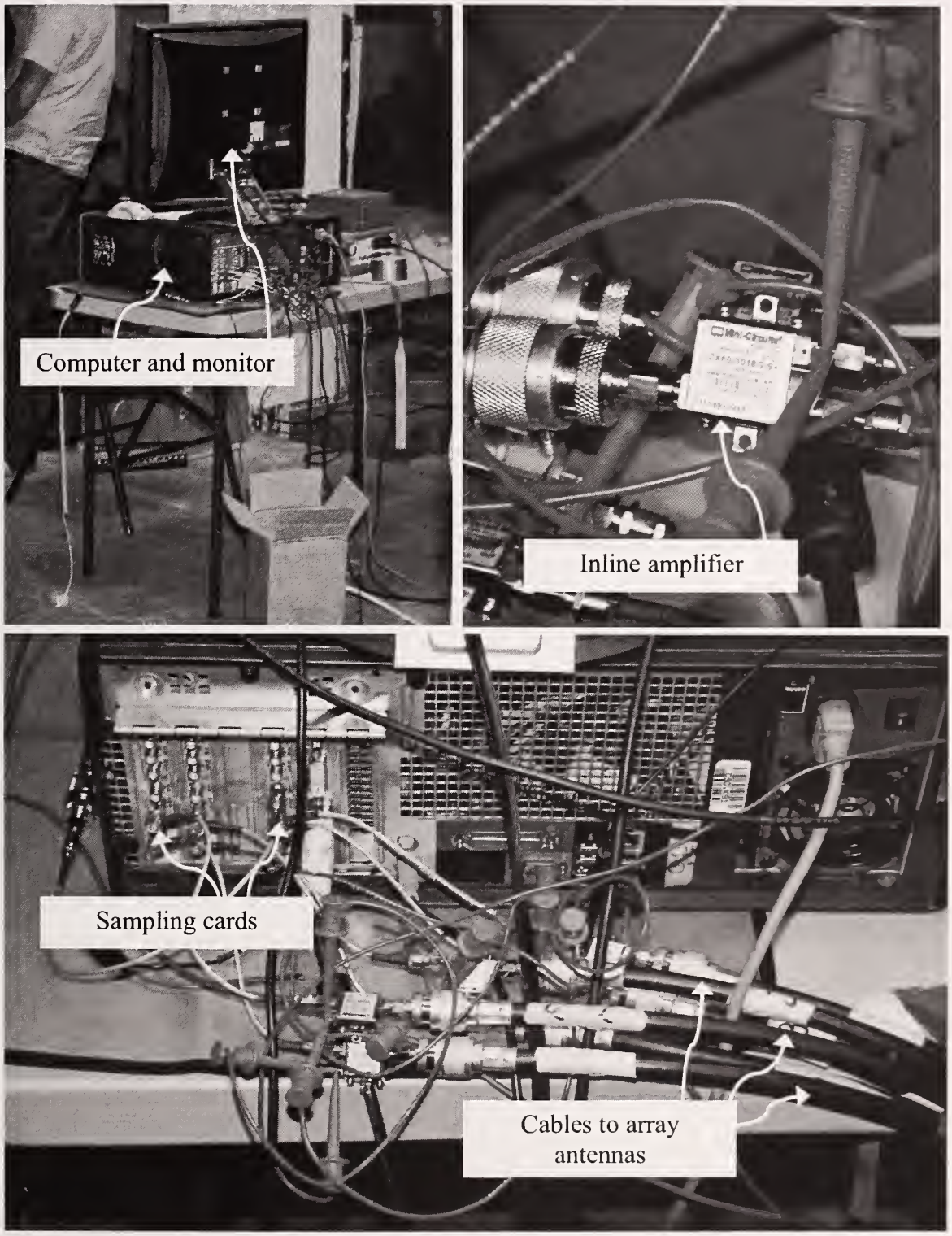

Figure 6. Measurement computer with sampling cards. Note that an in line amplifier provides approximately 20 dB of gain before the waveform is sampled.

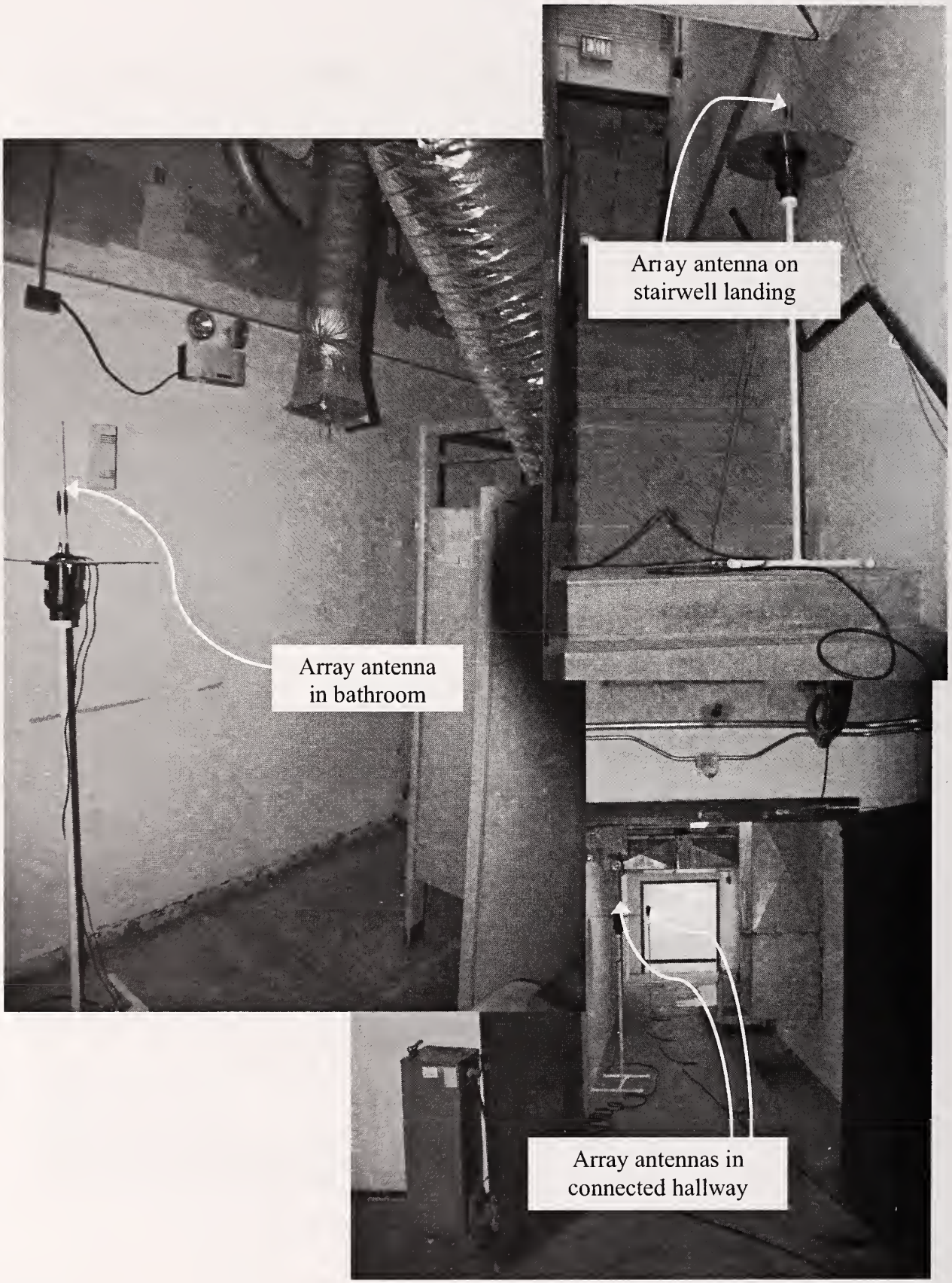

Figure 7. Some of the 750 MHz antenna array elements in the basement of Building 24.

Figure 8. Some of the antenna array elements used in the 750 MHz measurements carried out in Denver.

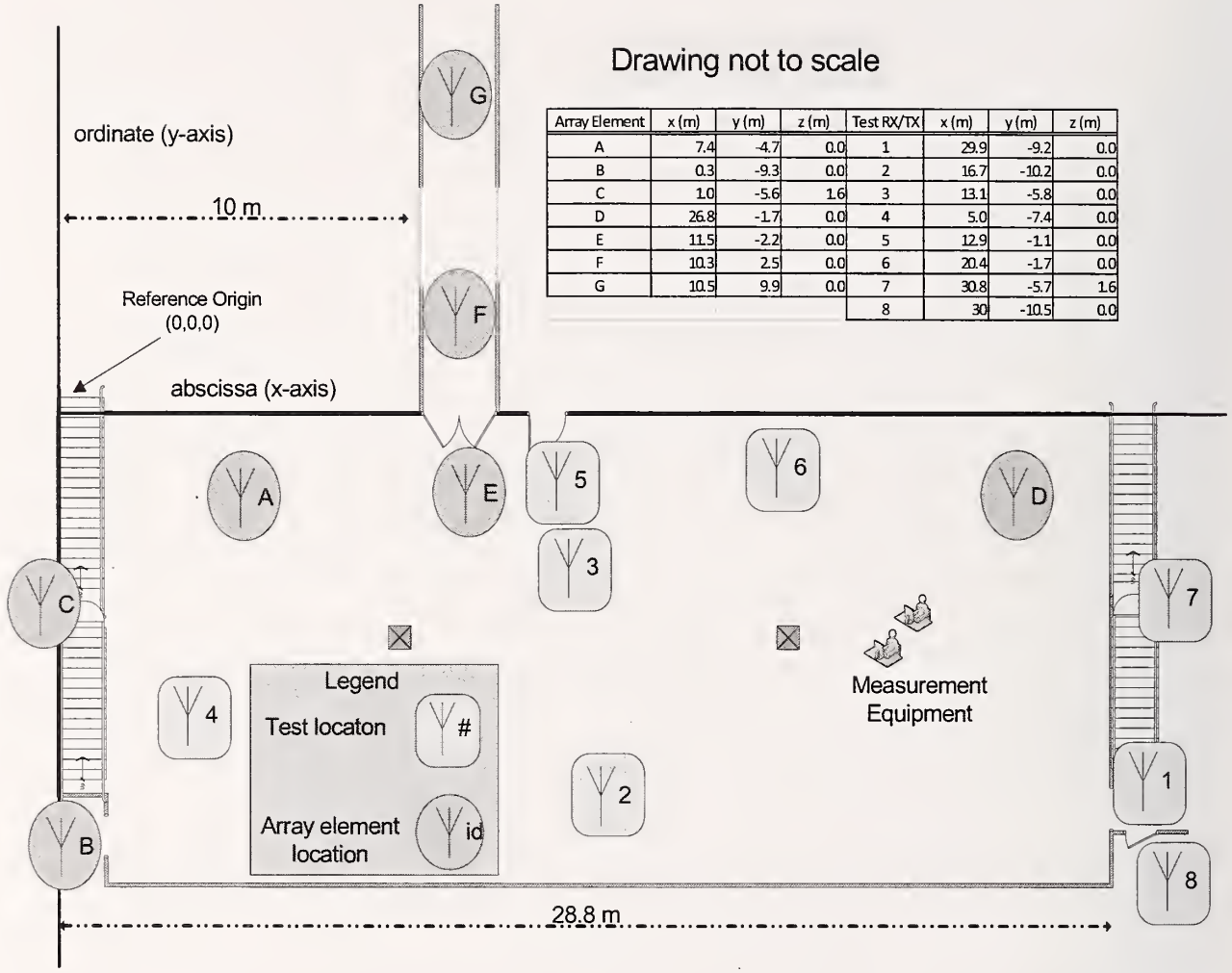

Array Element	x (m)	y (m)	z (m)	Test RX/TX	x (m)	y (m)	z (m)
A	7.4	-4.7	0.0	1	29.9	-9.2	0.0
B	0.3	-9.3	0.0	2	16.7	-10.2	0.0
C	1.0	-5.6	1.6	3	13.1	-5.8	0.0
D	26.8	-1.7	0.0	4	5.0	-7.4	0.0
E	11.5	-2.2	0.0	5	12.9	-1.1	0.0
F	10.3	2.5	0.0	6	20.4	-1.7	0.0
G	10.5	9.9	0.0	7	30.8	-5.7	1.6
				8	30	-10.5	0.0

Figure 9. Location of transmitter/receivers in the basement of Building 24 on the NIST, Boulder campus. The (x,y,z) values are given in the included table, with a non-zero value of z if the location is on one of the stair landings. The rectangular boxes contain testing locations and the ovals contain the *ad hoc* array elements.

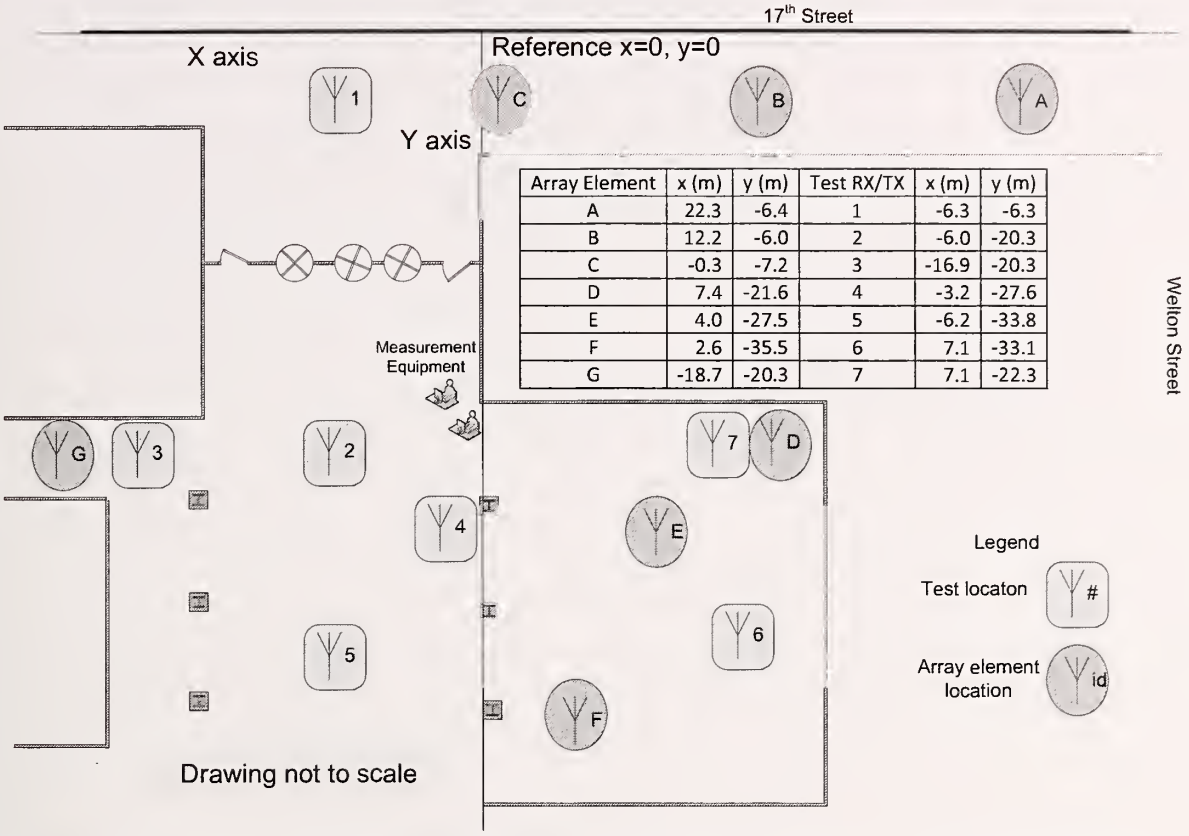

Array Element	x (m)	y (m)	Test RX/TX	x (m)	y (m)
A	22.3	-6.4	1	-6.3	-6.3
B	12.2	-6.0	2	-6.0	-20.3
C	-0.3	-7.2	3	-16.9	-20.3
D	7.4	-21.6	4	-3.2	-27.6
E	4.0	-27.5	5	-6.2	-33.8
F	2.6	-35.5	6	7.1	-33.1
G	-18.7	-20.3	7	7.1	-22.3

Figure 10. Location of transmitter/receivers at building in Denver, CO. The locations are given in (x,y) pairs. The rectangular boxes contain testing locations and the ovals contain the *ad hoc* array elements.

Appendix II: Experimental Results

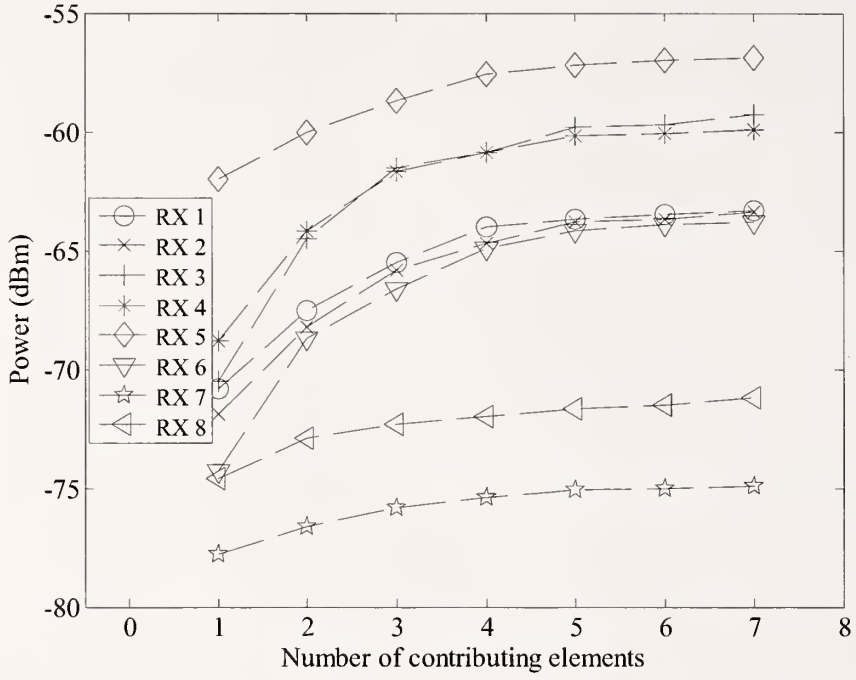

Figure 11. Building 24 raw results from spectrum analyzer measurements. Seven contributing transmitting antenna elements and eight receive antenna locations (RX#) were used.

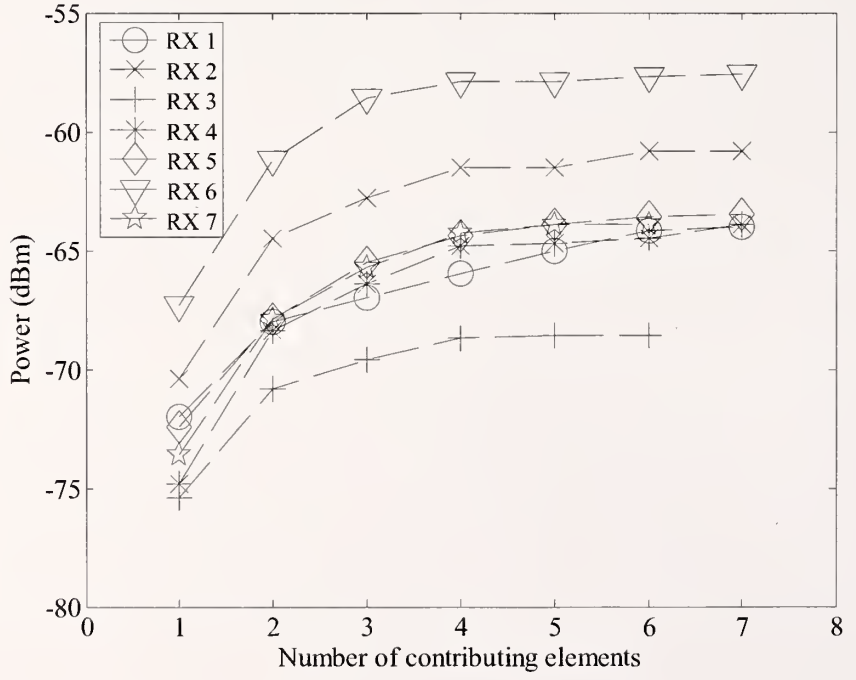

Figure 12. Denver raw results from spectrum analyzer measurements. Seven contributing transmitting antenna elements for five of the receive antenna locations, and six transmitting antenna elements for the other two receive location were used.

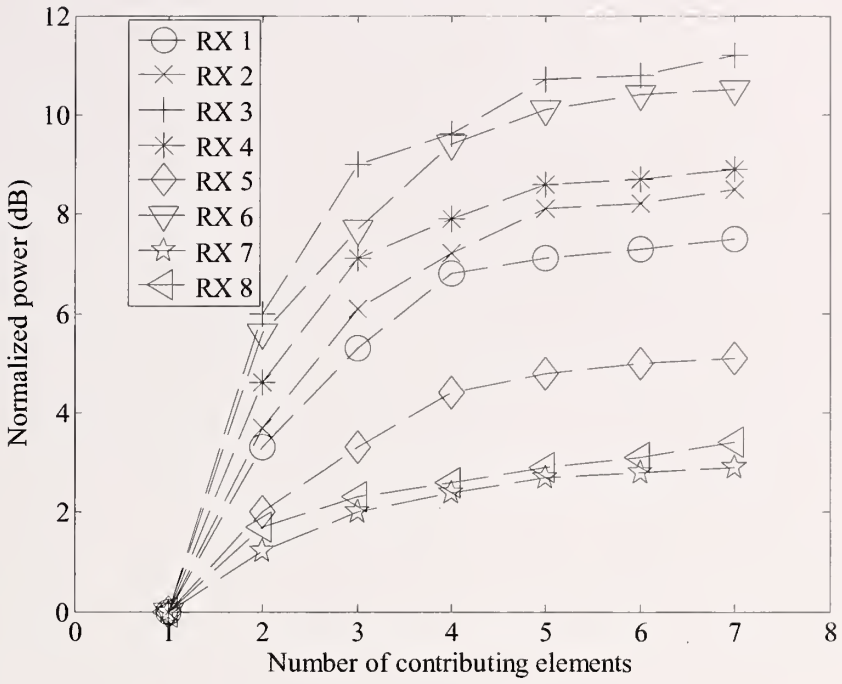

Figure 13. Building 24 cumulative sum of co-phased power. Power normalized by largest contributing element.

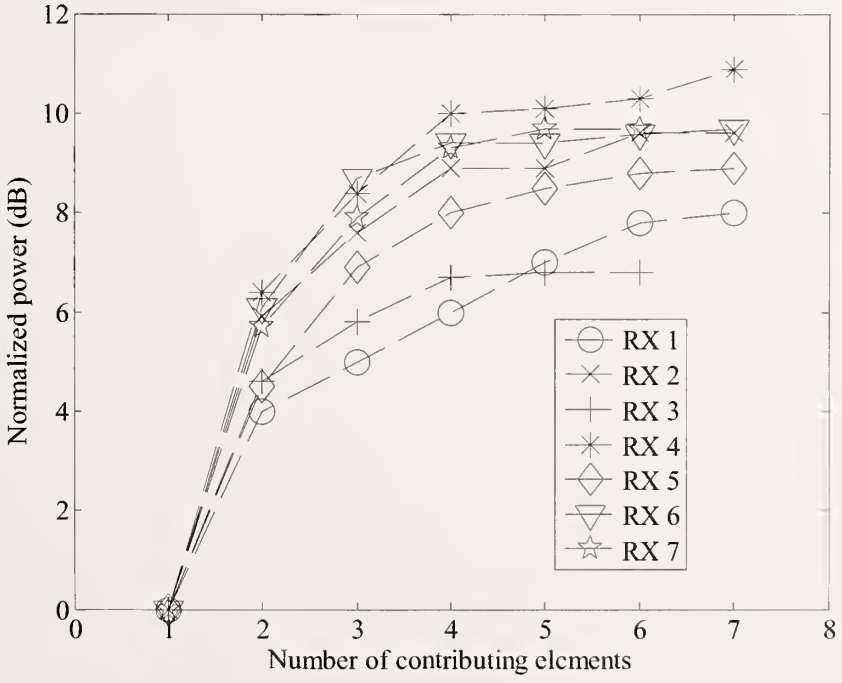

Figure 14. Denver cumulative sum of co-phased power, normalized by the largest contributing element. Two cases, RX 3 and RX 6, include only six transmitting elements.

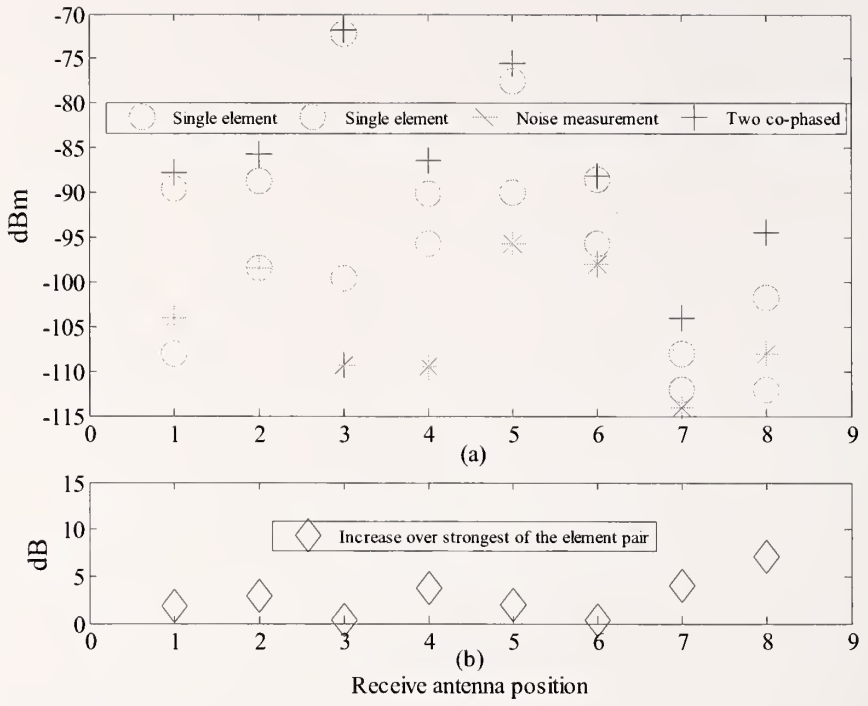

Figure 15. Building 24 results for two elements: (a) received power for single element, (b) increase in received power for two co-phased elements. Both elements were located in the hallway, off the main room.

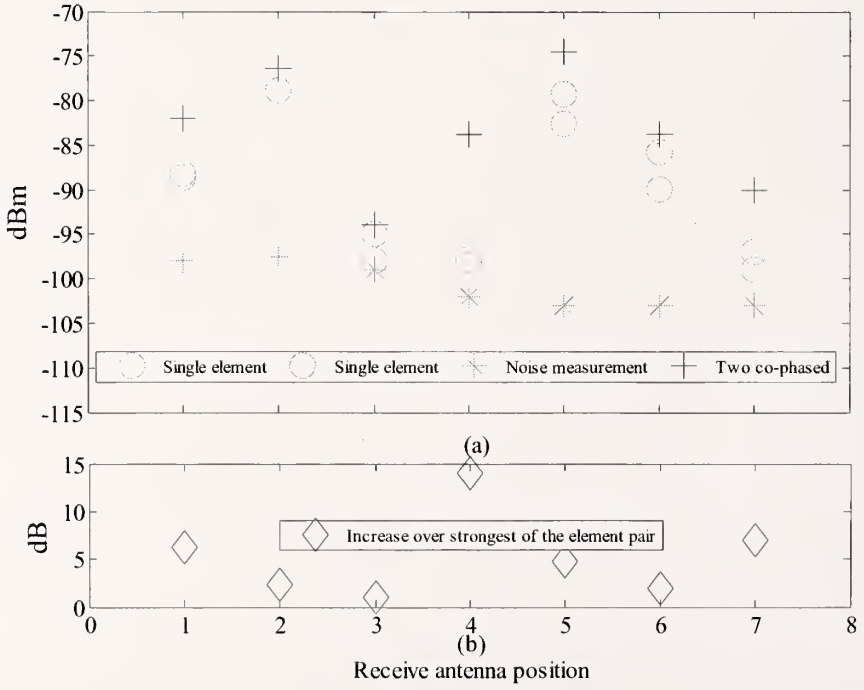

Figure 16. Denver results for two elements: (a) received power for single element, (b) increase in received power for two co-phased elements. Two of the weaker elements were selected, but not necessarily the weakest two.

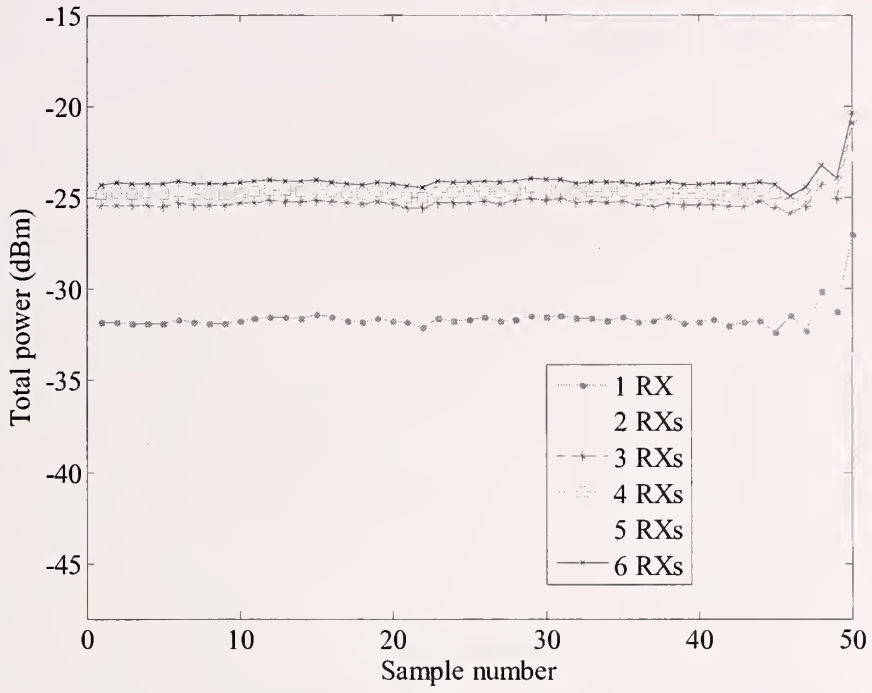

Figure 17. Building 24, absolute value of co-phased cumulative sum; TX position 1.

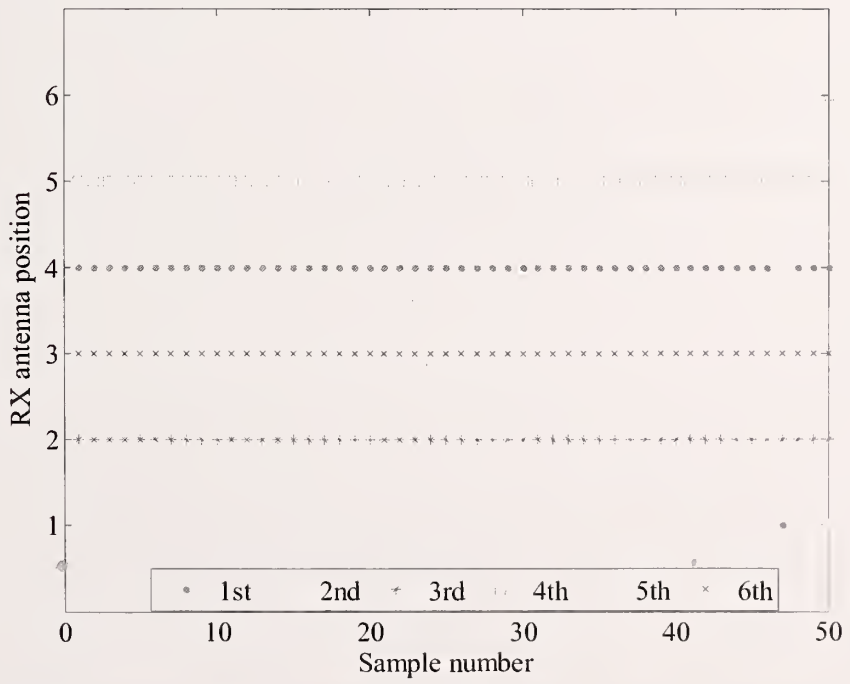

Figure18. Building 24, TX position 1. RX order in the co-phased summation.

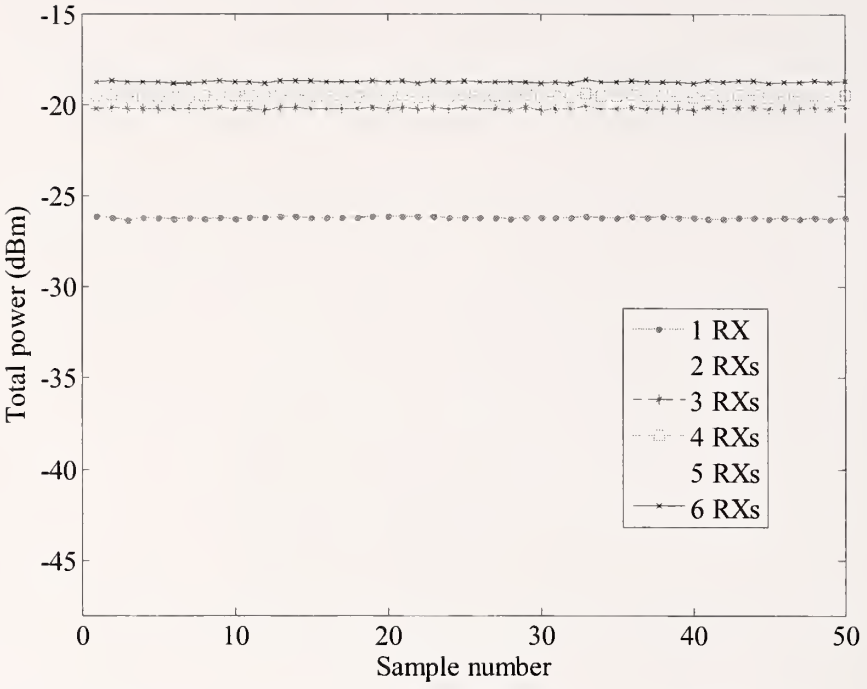

Figure 19. Building 24, absolute value of co-phased cumulative sum; TX position 2.

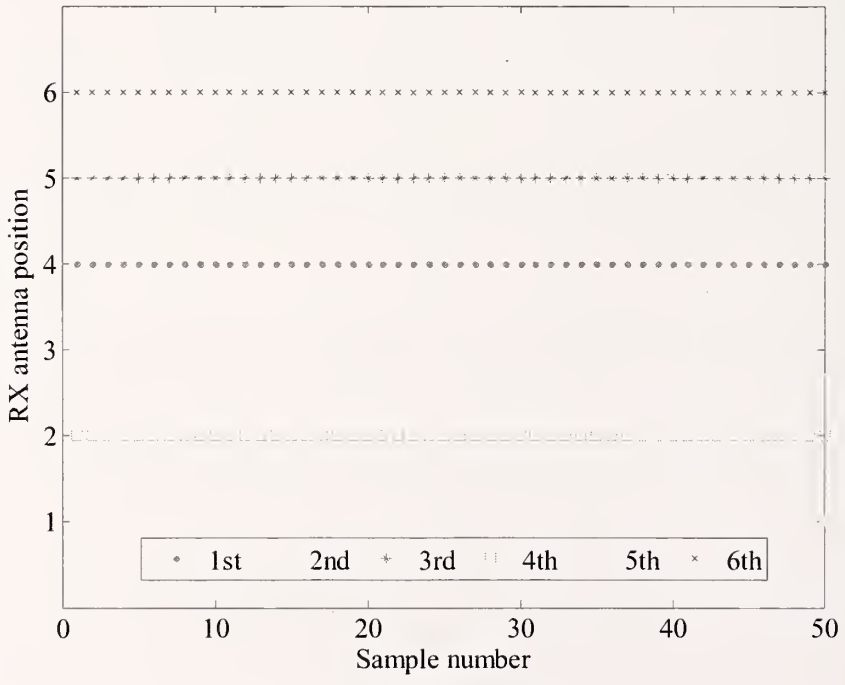

Figure 20. Building 24, TX position 2. RX order in the co-phased summation.

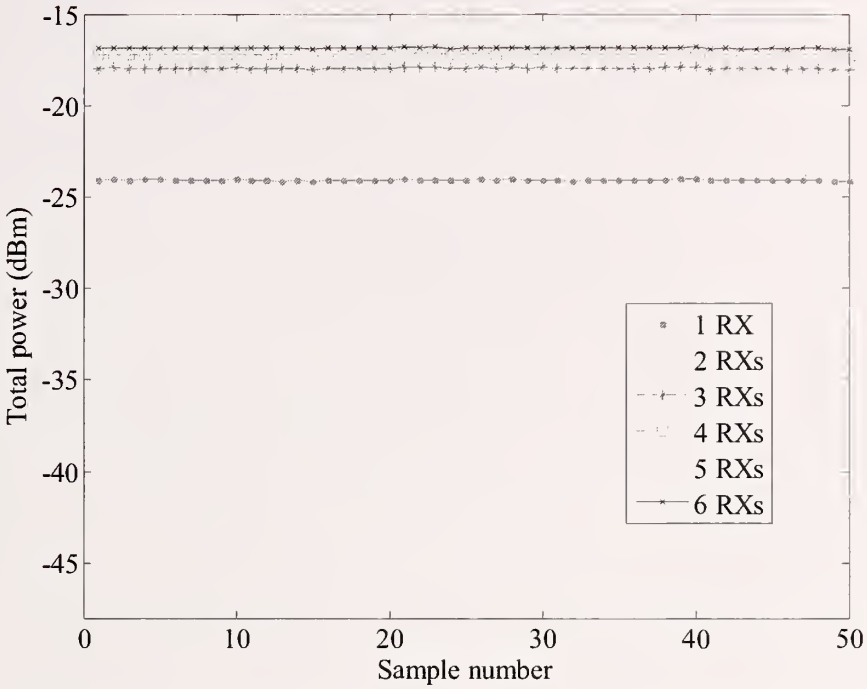

Figure 21. Building 24, absolute value of co-phased cumulative sum; TX position 3.

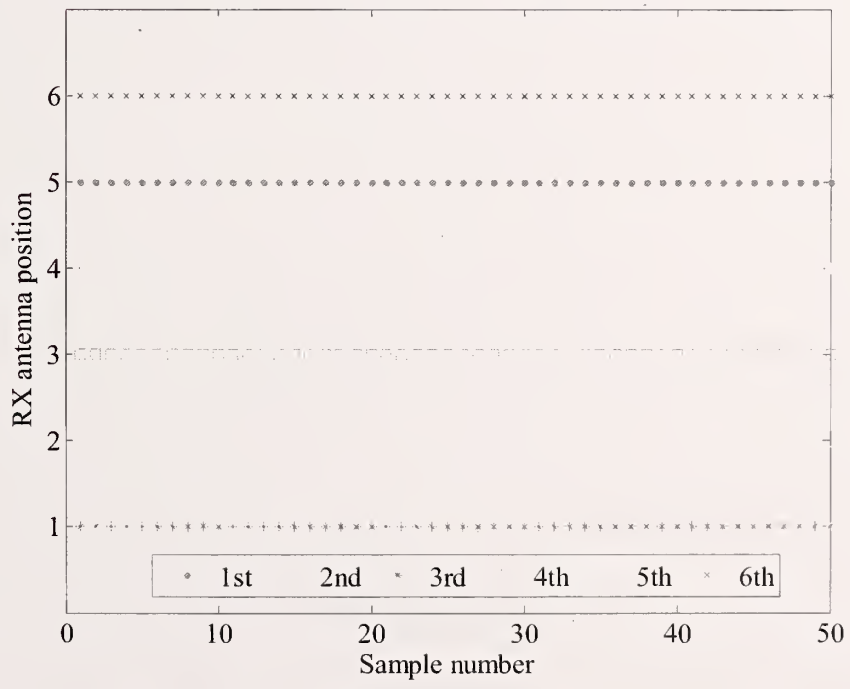

Figure 22. Building 24, TX position 3. RX order in the co-phased summation.

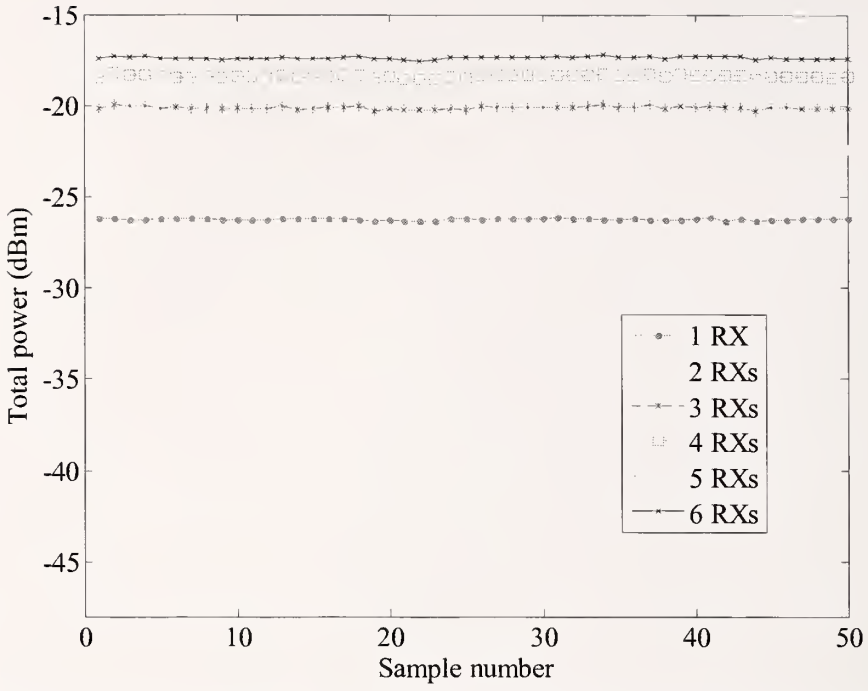

Figure 23. Building 24, absolute value of co-phased cumulative sum; TX position 4.

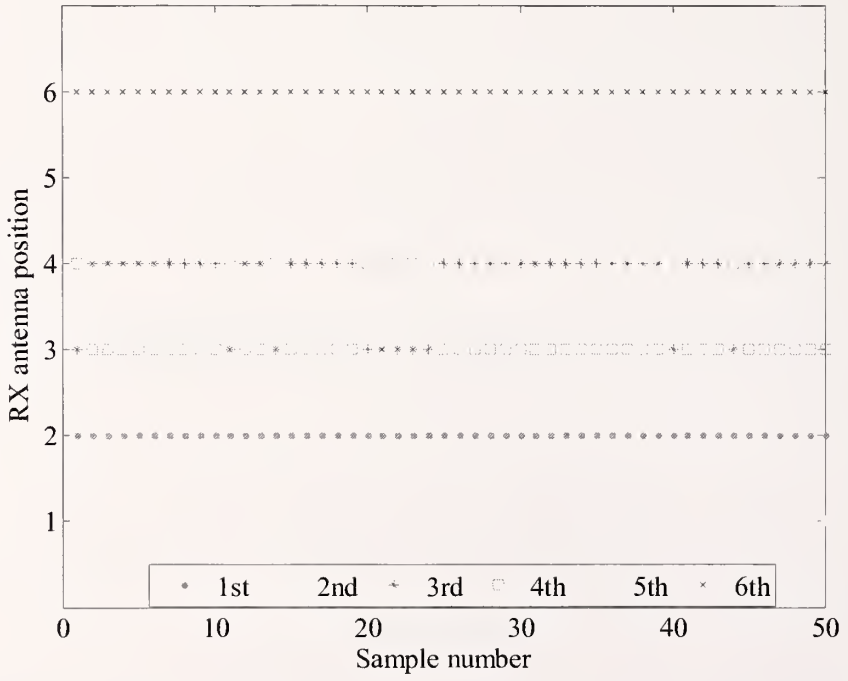

Figure 24. Building 24, TX position 4. RX order in the co-phased summation.

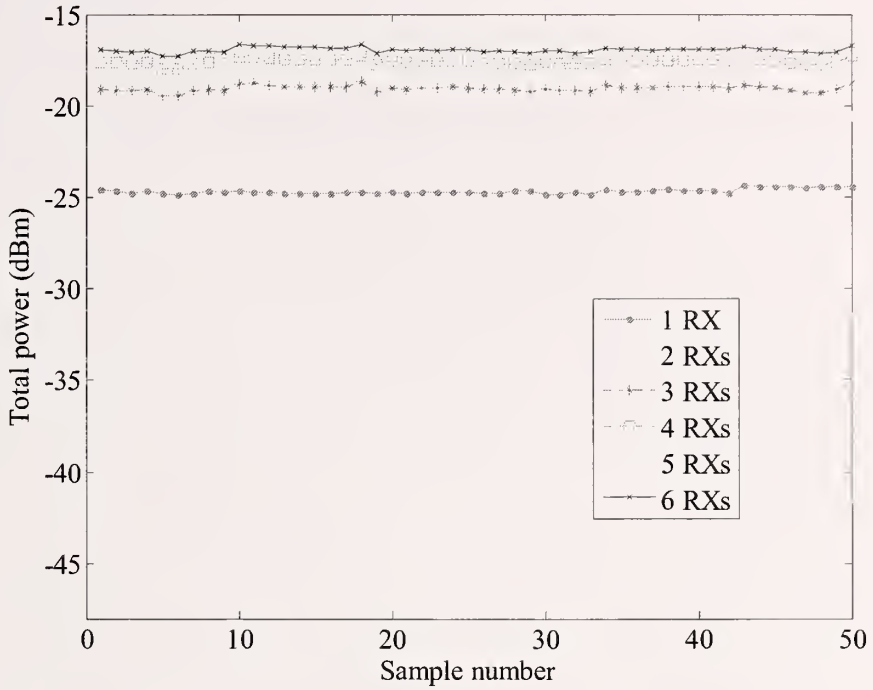

Figure 25. Building 24, absolute value of co-phased cumulative sum; TX position 5.

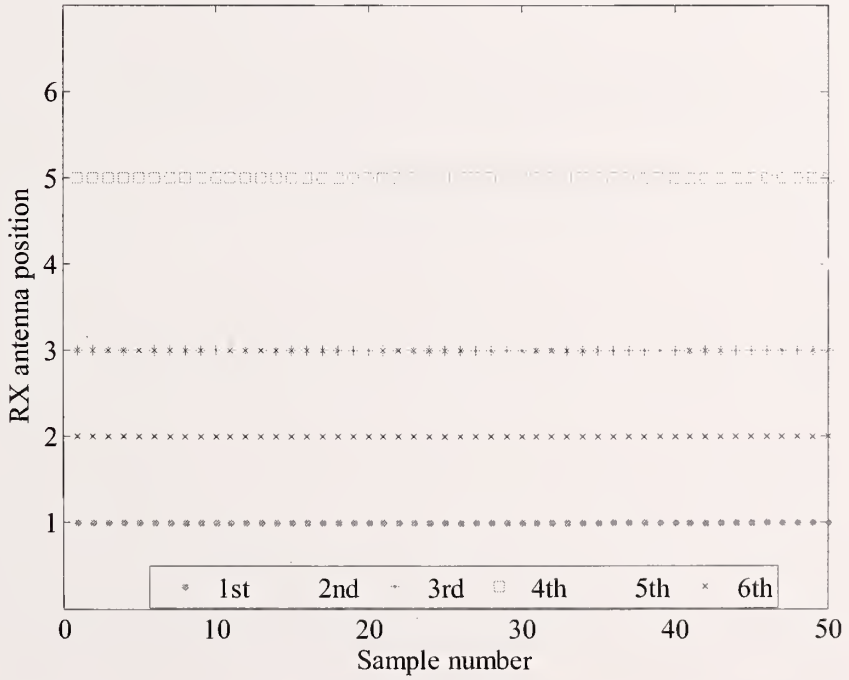

Figure 26. Building 24, TX position 5. RX order in the co-phased summation.

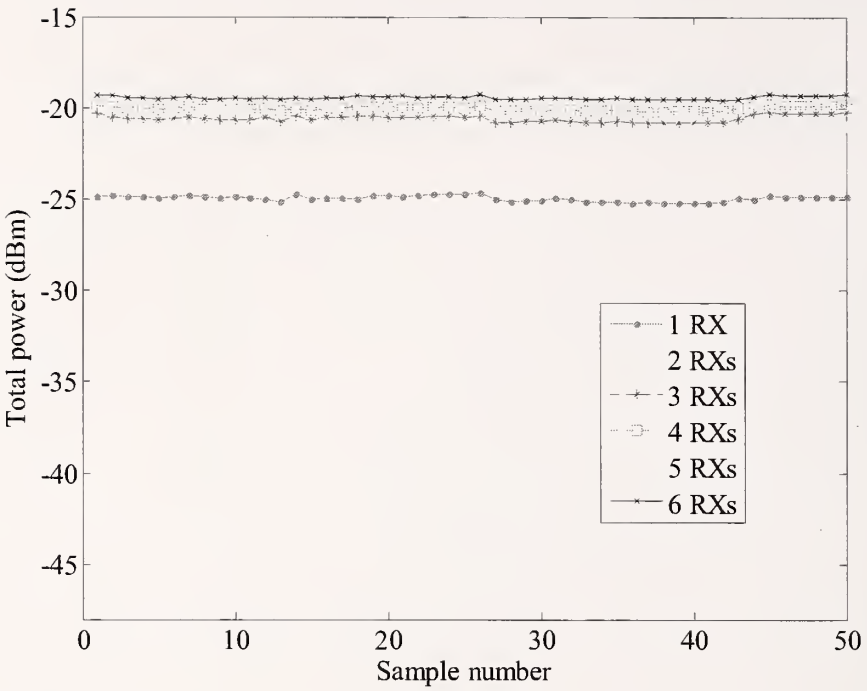

Figure 27. Building 24, absolute value of co-phased cumulative sum; TX position 6.

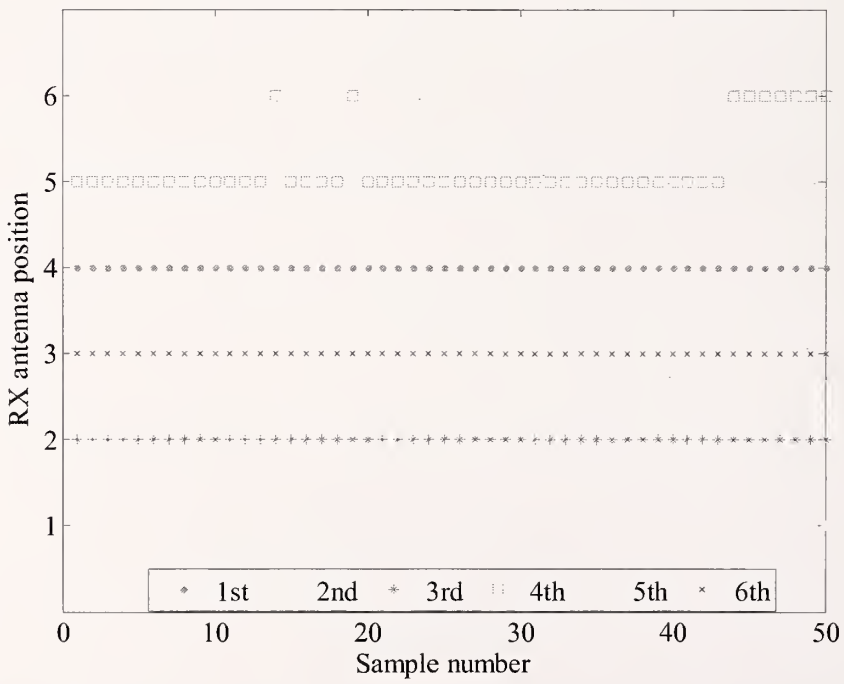

Figure 28. Building 24, TX position 6. RX order in the co-phased summation.

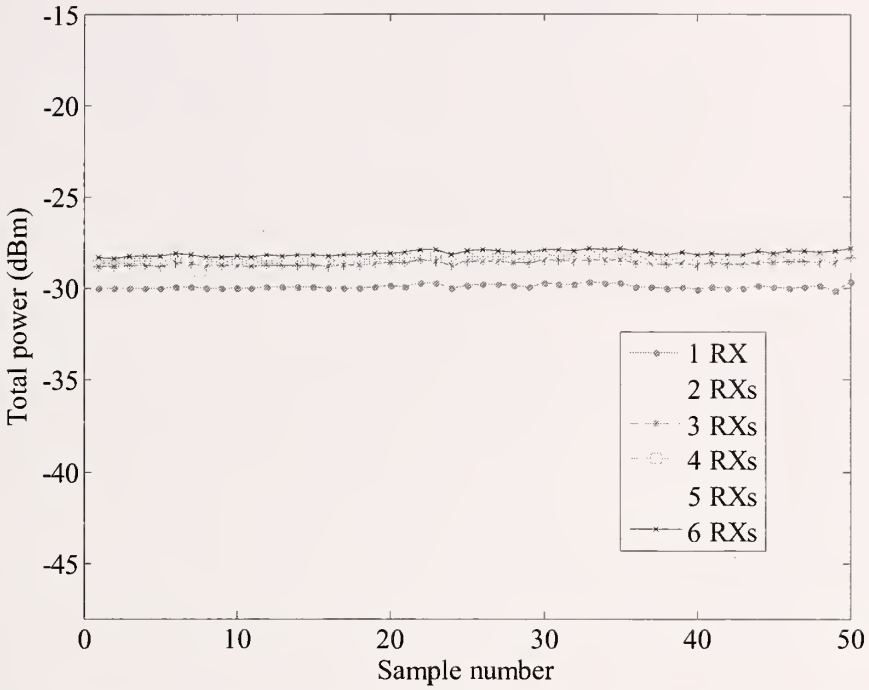

Figure 29. Building 24, absolute value of co-phased cumulative sum; TX position 7.

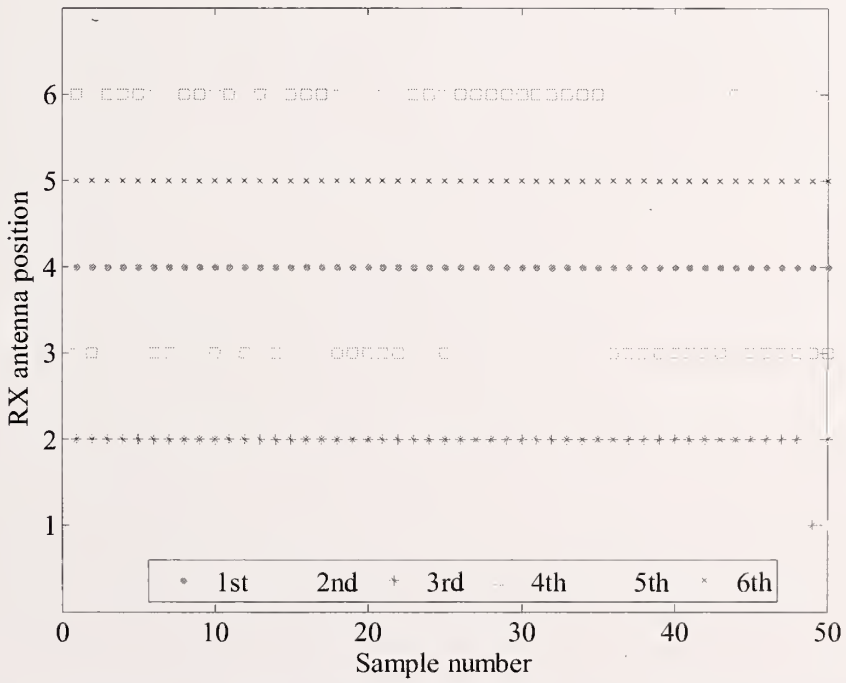

Figure 30. Building 24, TX position 7. RX order in the co-phased summation.

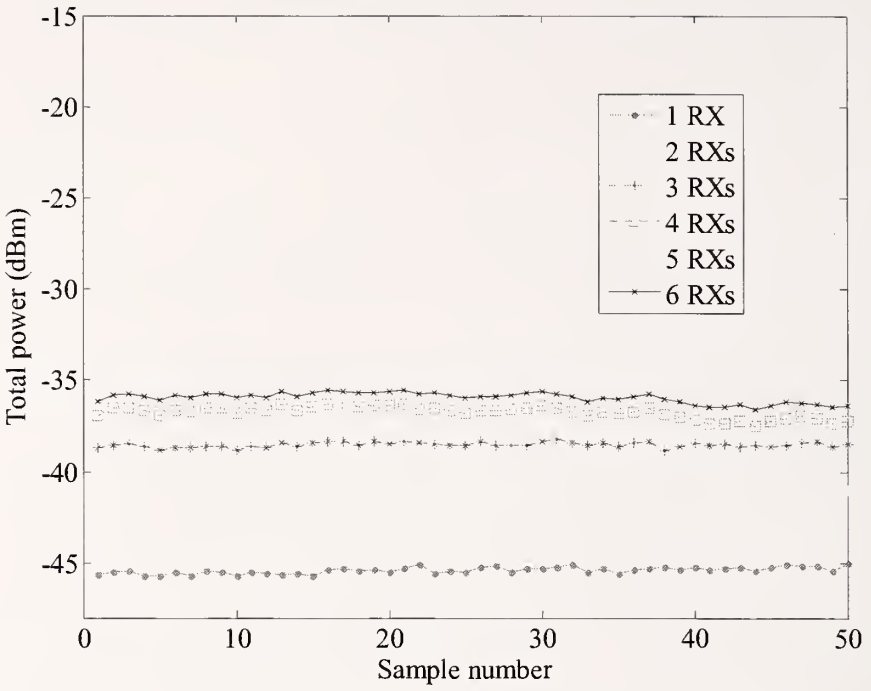

Figure 31. Building 24, absolute value of co-phased cumulative sum; TX position 8.

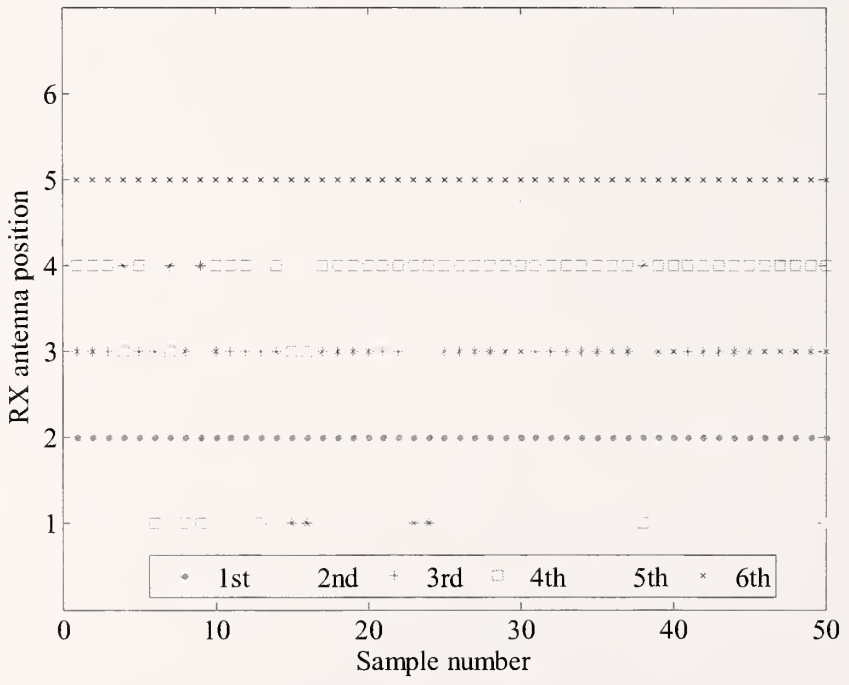

Figure 32. Building 24, TX position 8. RX order in the co-phased summation.

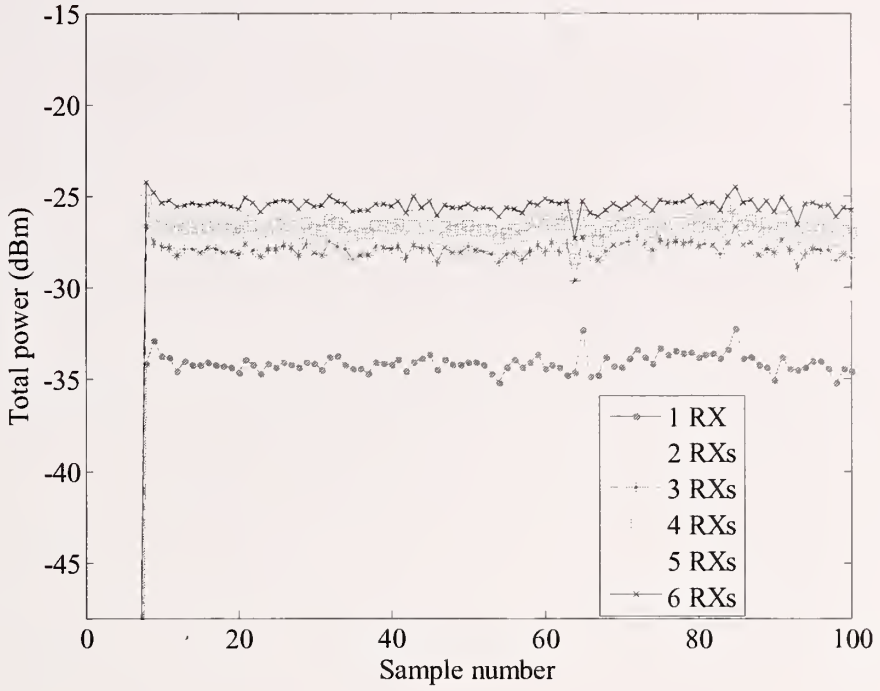

Figure 33. Denver Building, absolute value of co-phased cumulative sum; TX position 1.

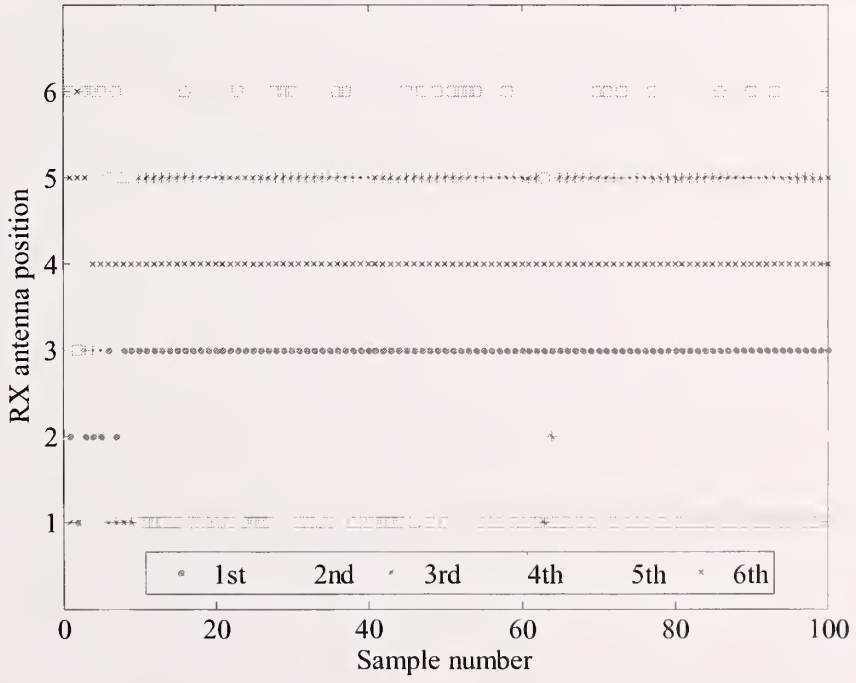

Figure 34. Denver Building., TX position 1. RX order in the co-phased summation.

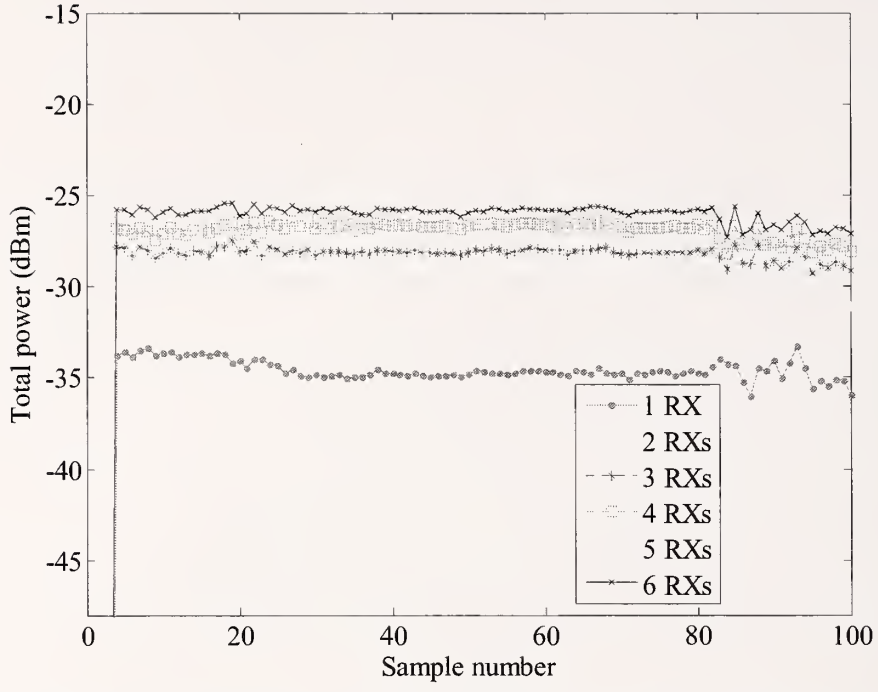

Figure 35. Denver Building, absolute value of co-phased cumulative sum; TX position 2.

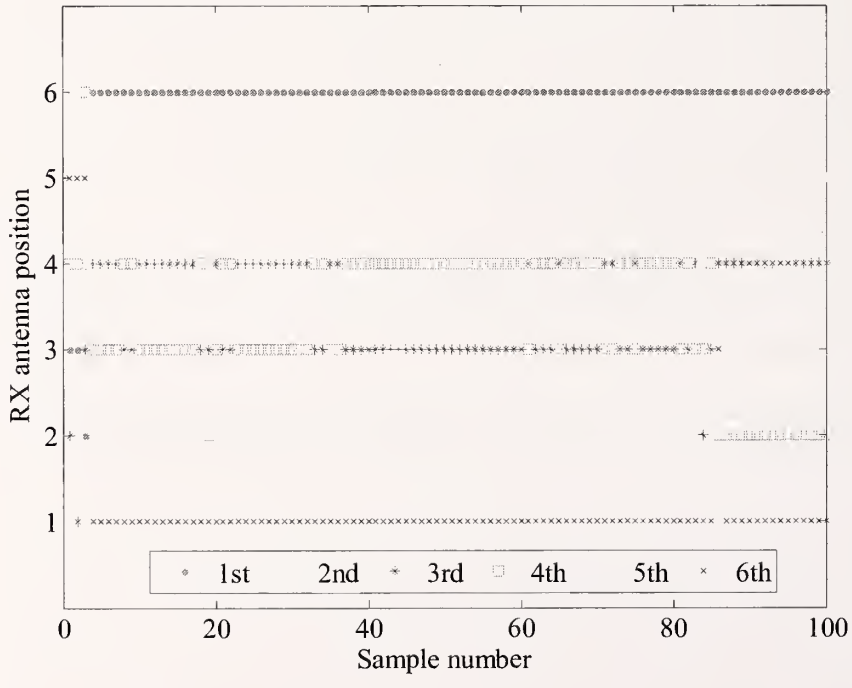

Figure 36. Denver Building, TX position 2. RX order in the co-phased summation.

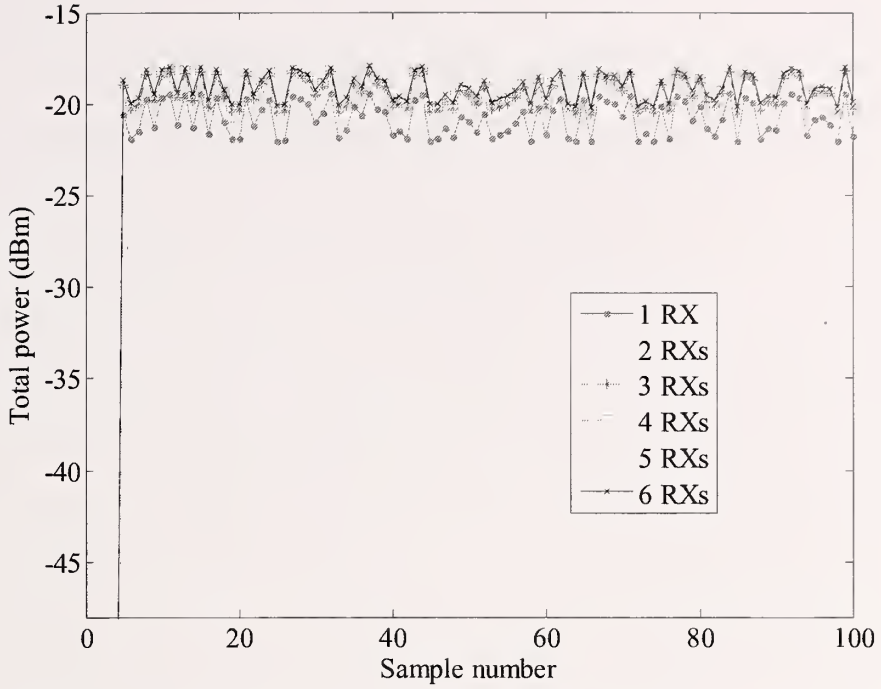

Figure 37. Denver Building, absolute value of co-phased cumulative sum; TX position 3.

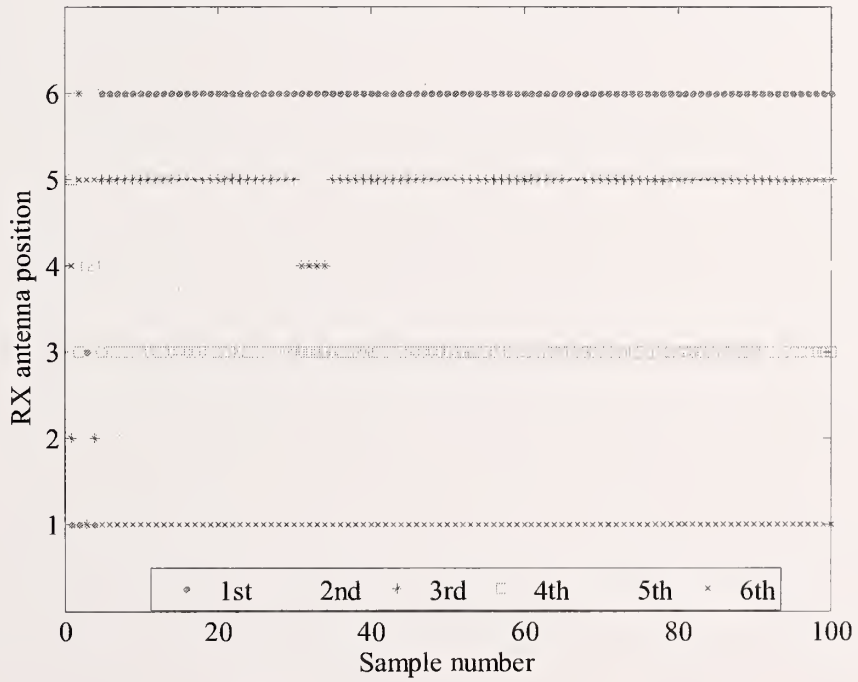

Figure 38. Denver Building, TX position 3. RX order in the co-phased summation.

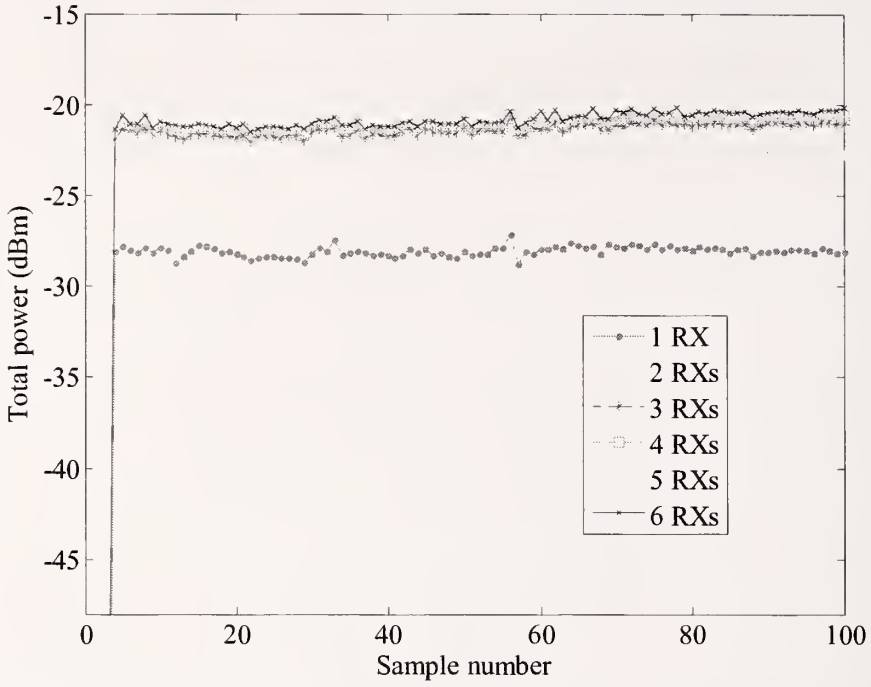

Figure 39. Denver Building, absolute value of co-phased cumulative sum; TX position 4.

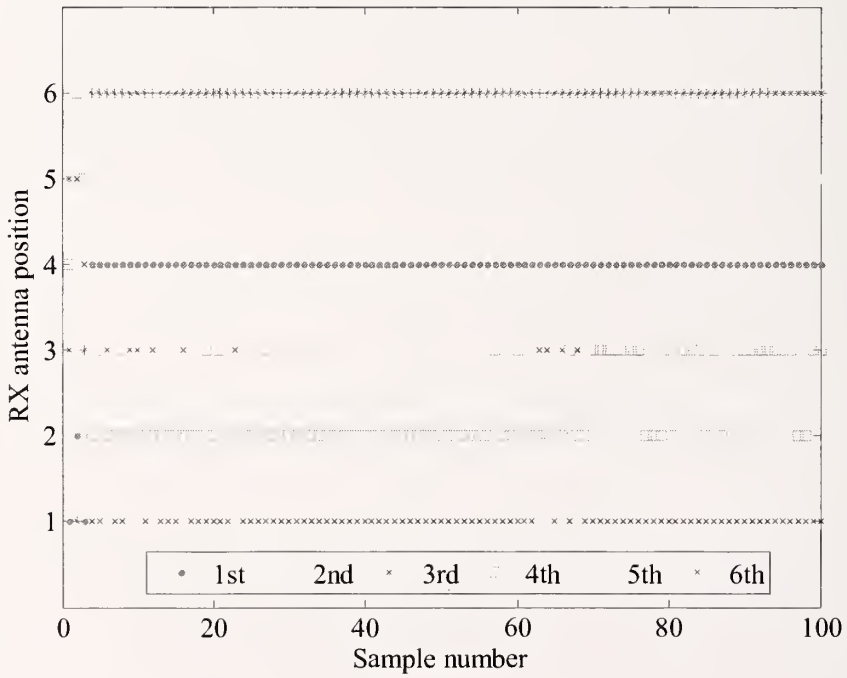

Figure 40. Denver Building, TX position 4. RX order in the co-phased summation.

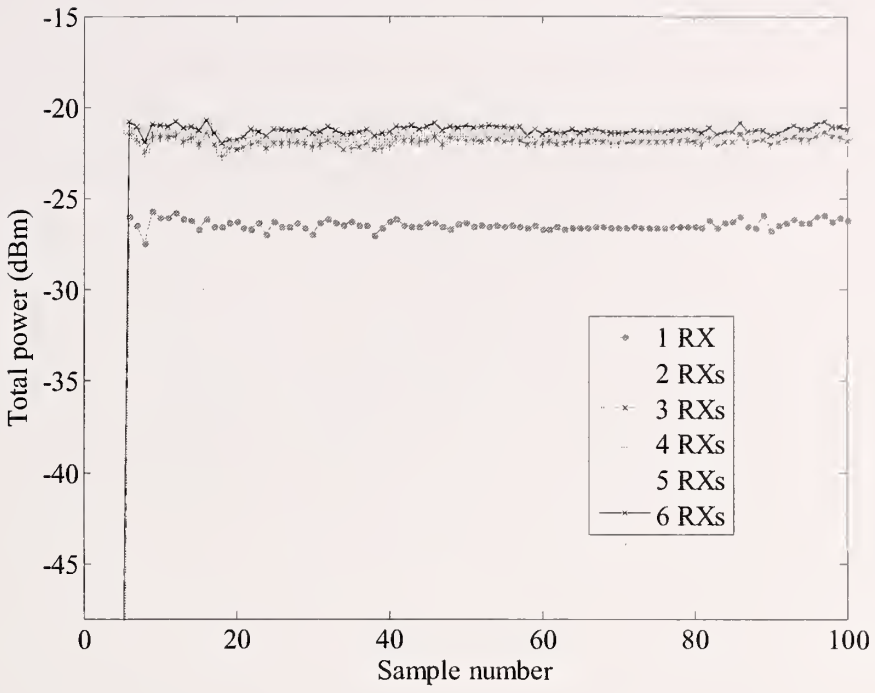

Figure 41. Denver Building, absolute value of co-phased cumulative sum; TX position 5.

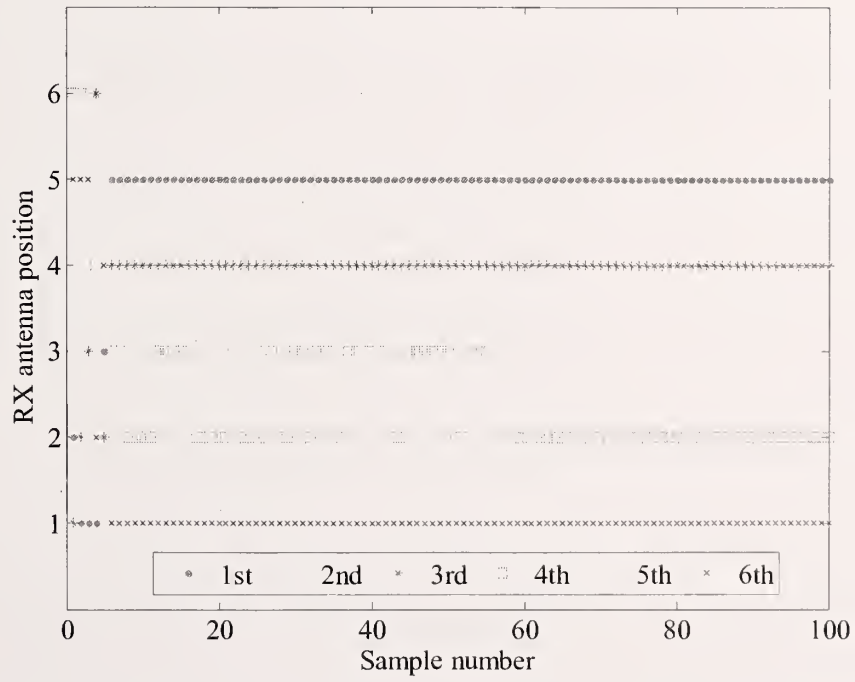

Figure 42. Denver Building, TX position 5. RX order in the co-phased summation.

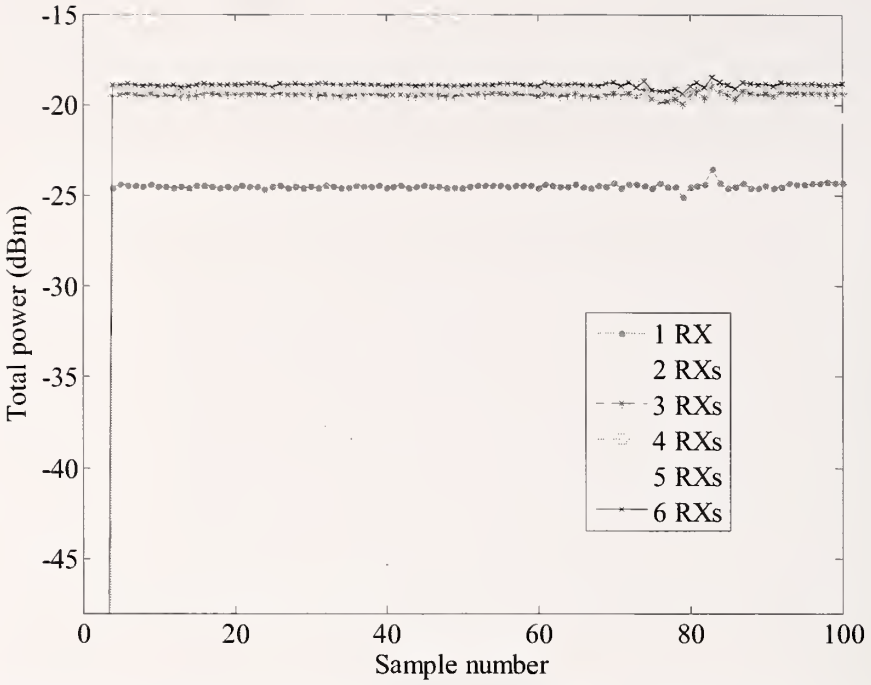

Figure 43. Denver Building, absolute value of co-phased cumulative sum; TX position 6.

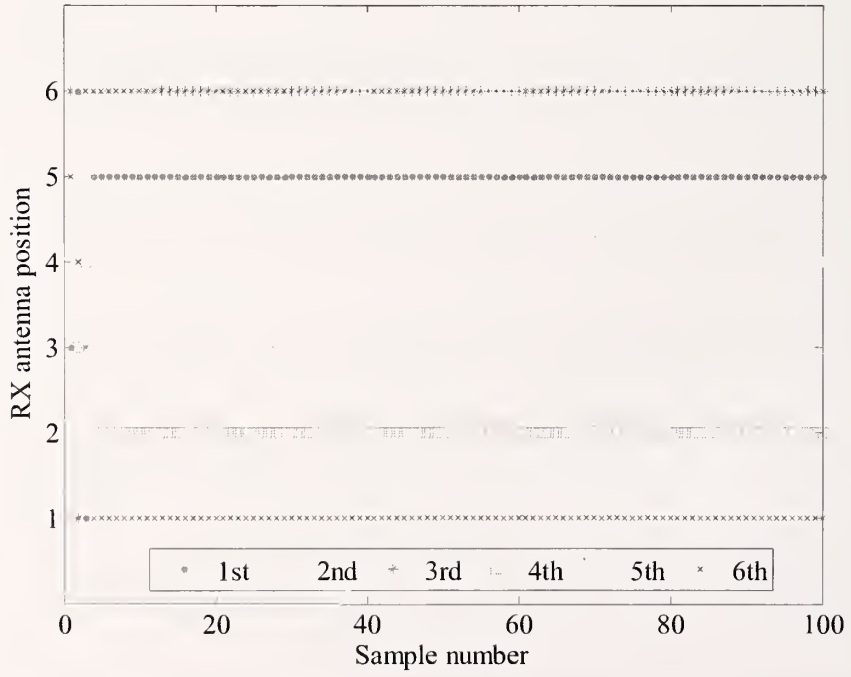

Figure 44. Denver Building, TX position 6. RX order in the co-phased summation.

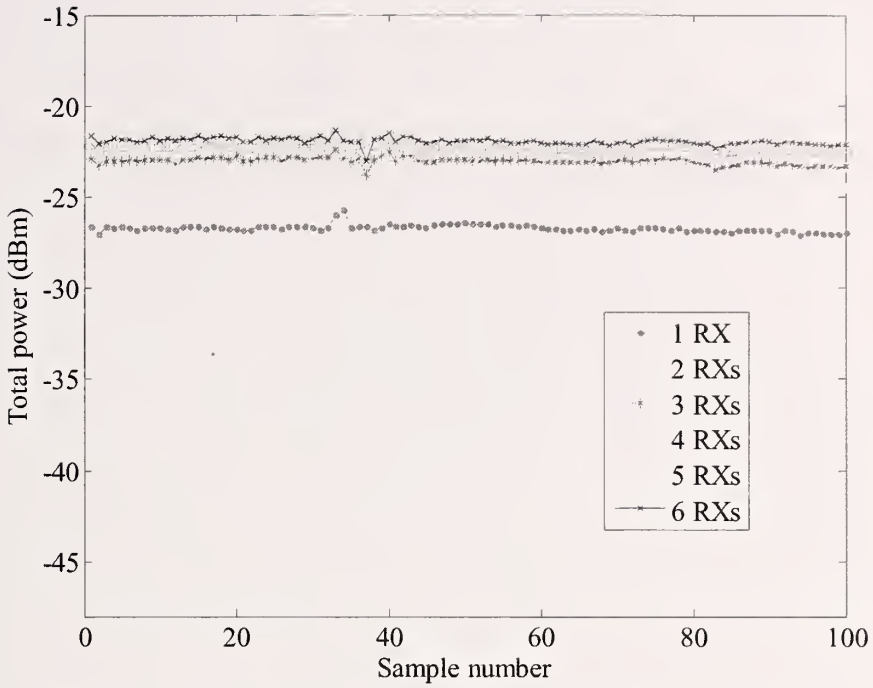

Figure 45. Denver Building, absolute value of co-phased cumulative sum; TX position 7.

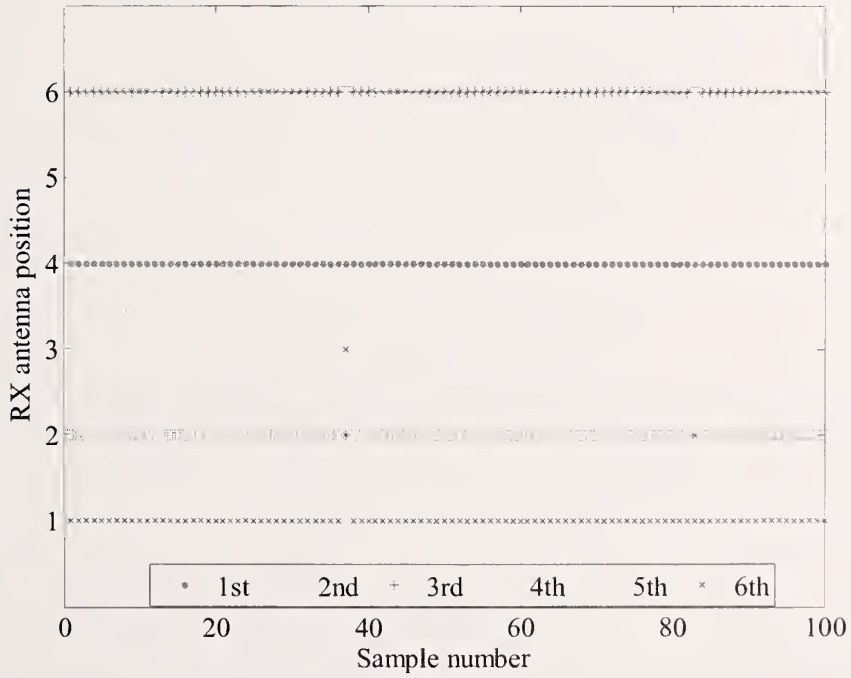

Figure 46. Denver Building, TX position 7. RX order in the co-phased summation.

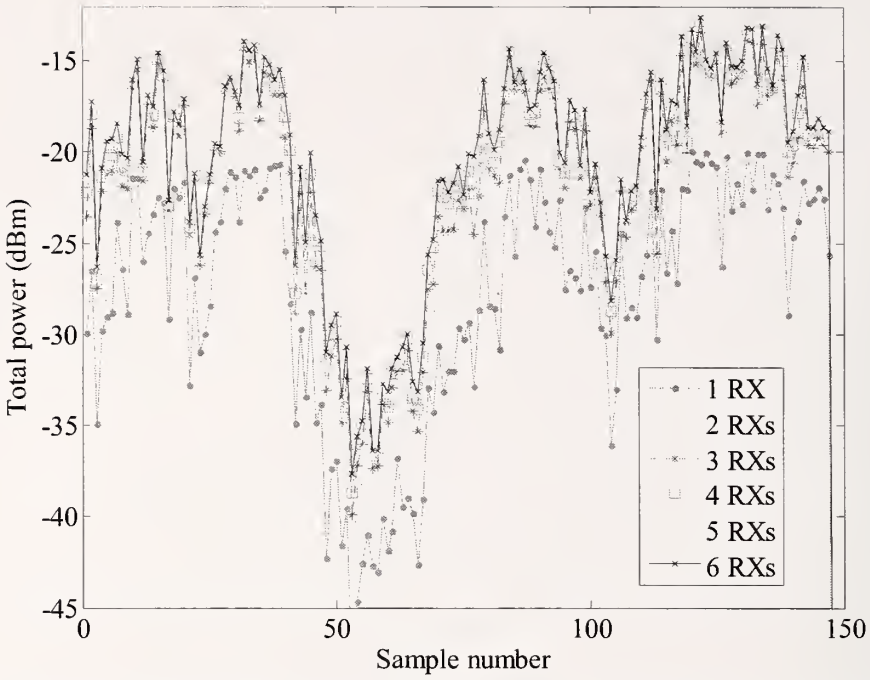

Figure 47. Denver Building, absolute value of co-phased cumulative sum. Transmitter carried over path both inside and outside of the *ad hoc* array. Note that the vertical scale is increased by 3 dB over previous Denver plots, e.g., compared to the vertical scale in Figure.

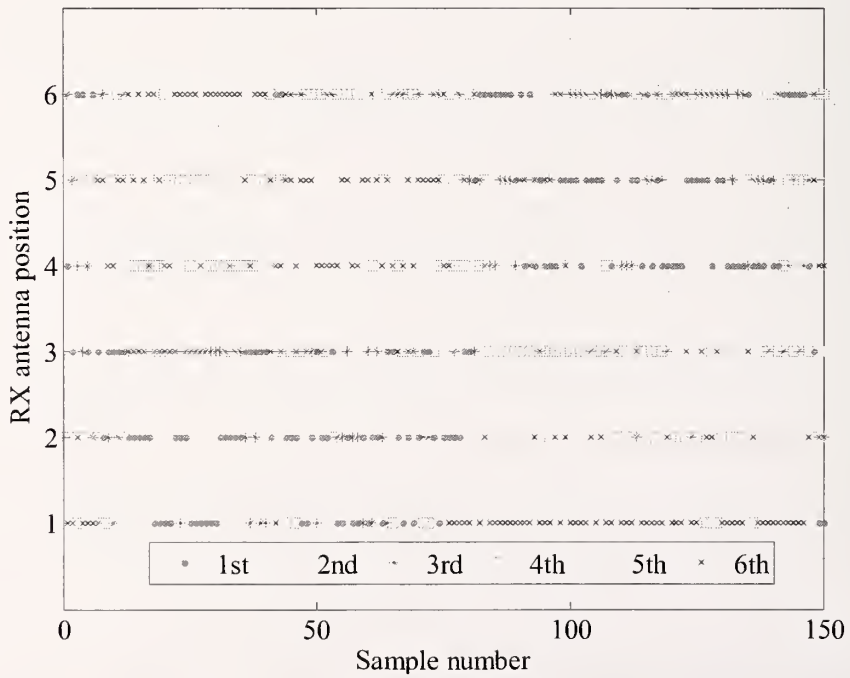

Figure 48. Denver Building, TX carried over path both inside and outside of the *ad hoc* array. RX order in the co-phased summation.

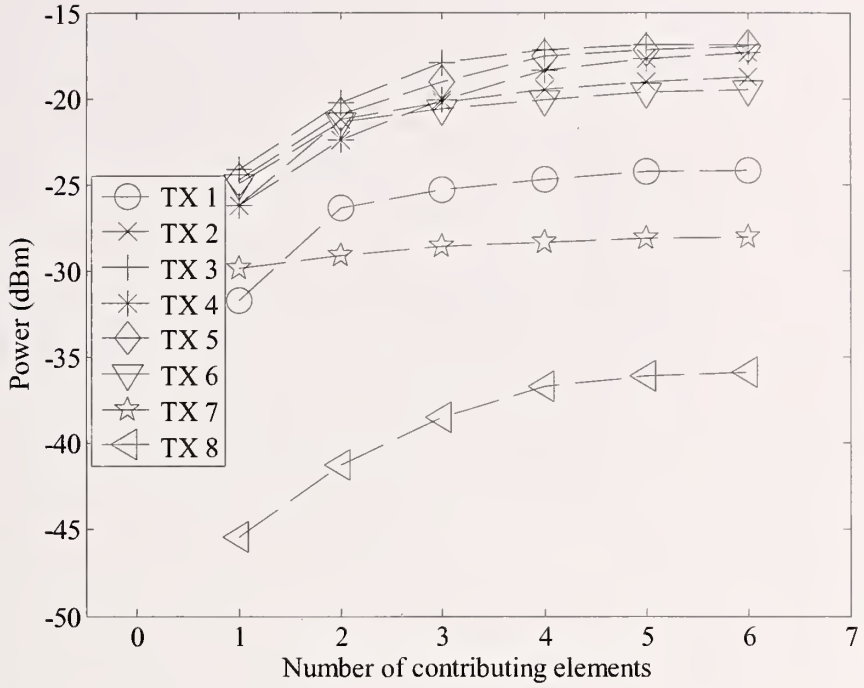

Figure 49. Building 24 raw average cumulative power results based on 41 samples. TX number refers to the transmitter position, which is the same as the RX position used in the spectrum analyzer measurements.

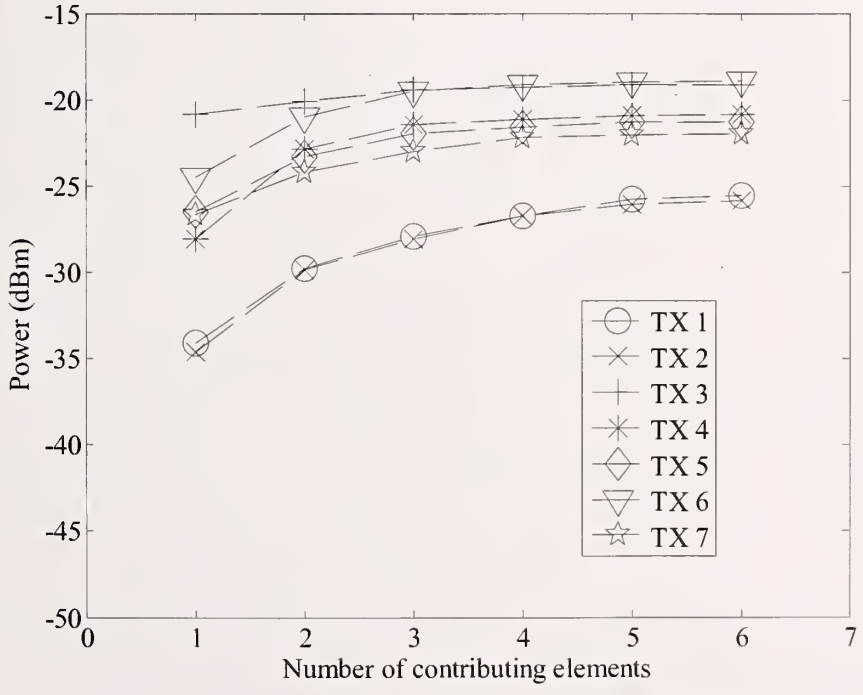

Figure 50. Denver raw average cumulative power results based on 71 samples. TX number refers to the transmitter position, which is the same as the RX position used in the spectrum analyzer measurements.

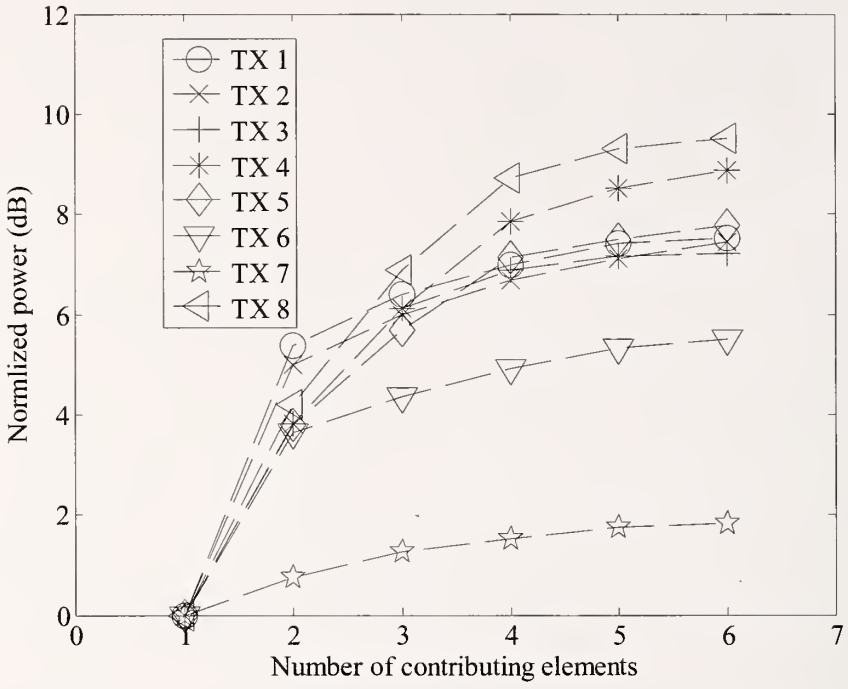

Figure 51. Building 24 average cumulative power results based on 41 samples, normalized by the largest contributing element. TX number refers to the transmitter position, which is the same as the RX position used in the spectrum analyzer measurements.

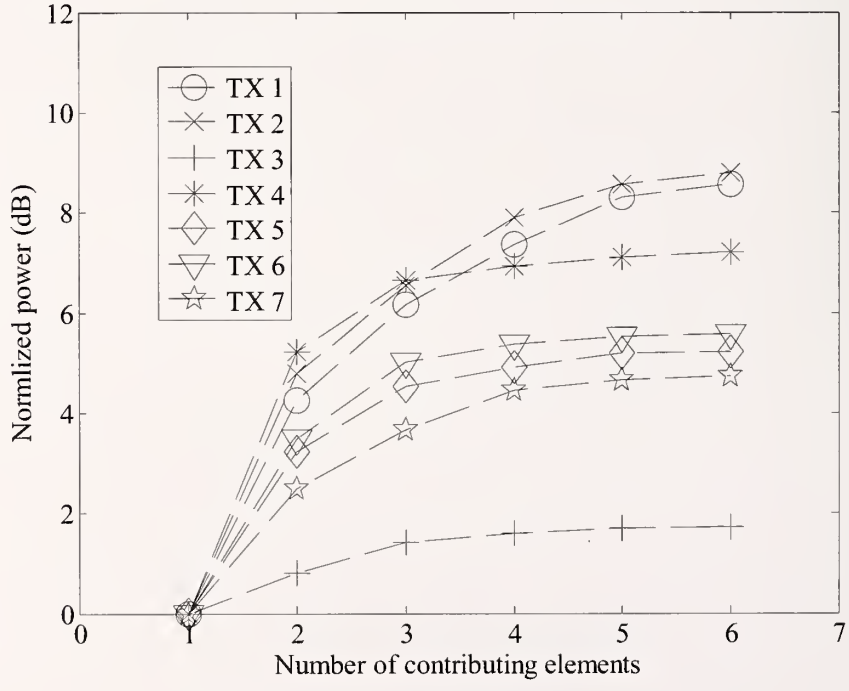

Figure 52. Denver average cumulative power results based on 71 samples, normalized by the largest contributing element. TX number refers to the transmitter position, which is the same as the RX position used in the spectrum analyzer measurements.

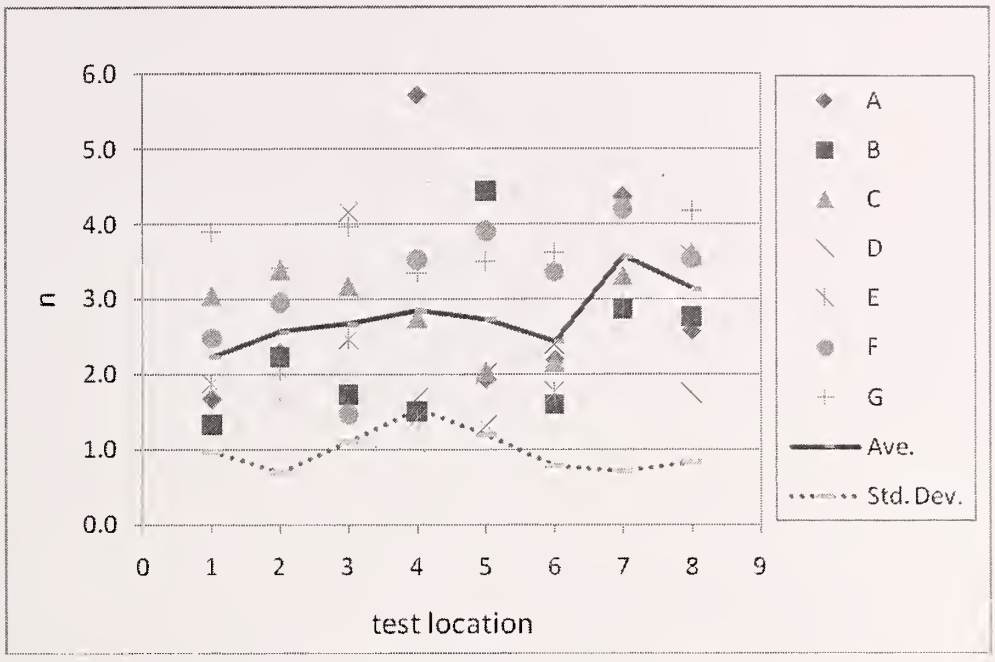

Figure 53. Building 24, 2.4 GHz path loss exponent for test locations 1 to 8, and array element A through G.

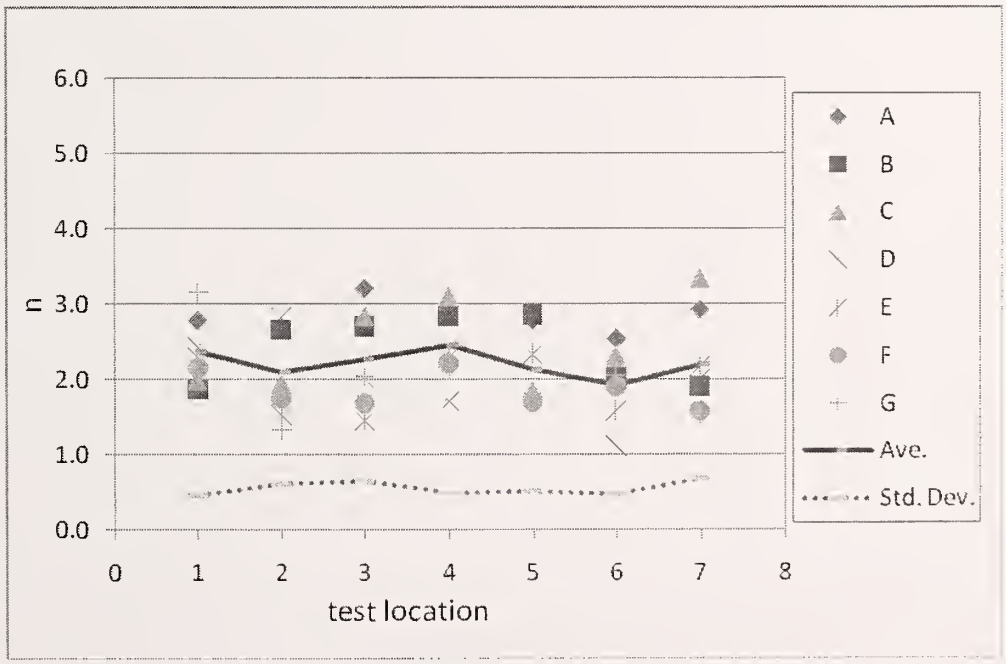

Figure 54. Denver building, 2.4 GHz path loss exponent for test locations 1 to 7, and array element A through G.

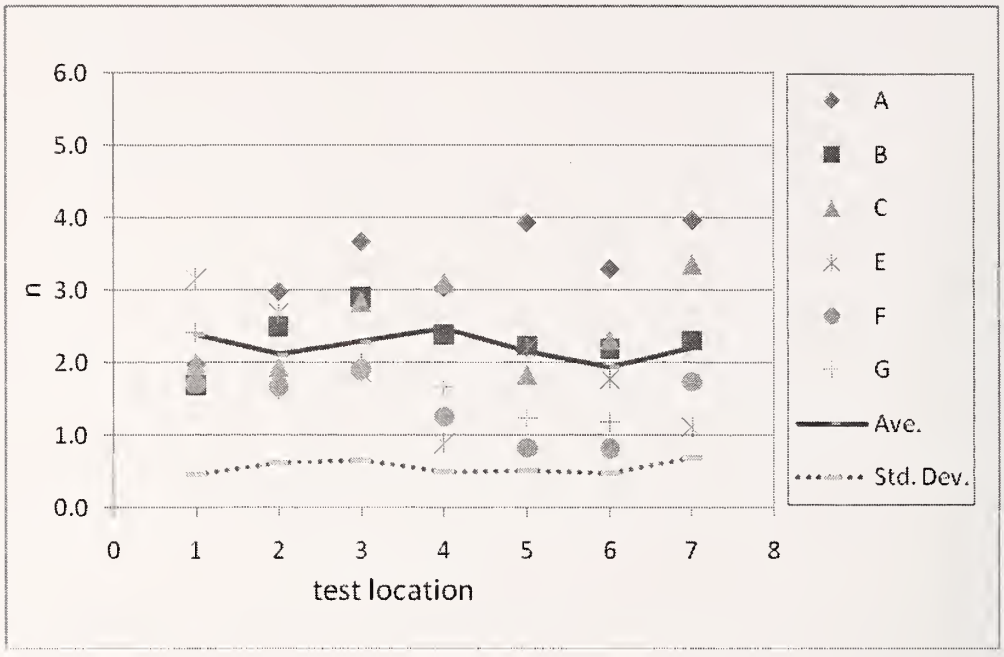

Figure 55. Denver building, 750 MHz path loss exponent results. Note that array element "D" is not included because only six channels are sampled with the computer and sampling card system.

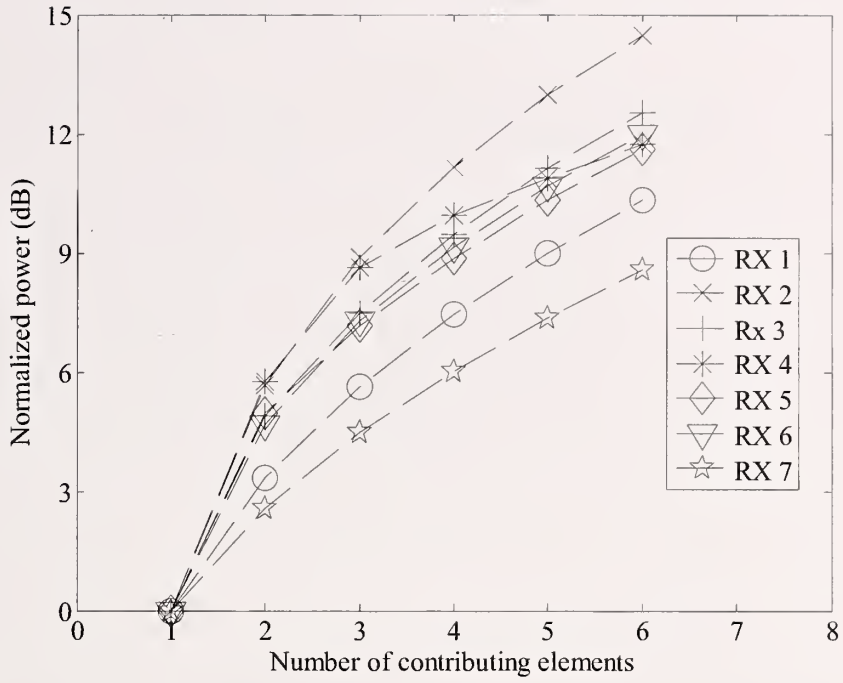

Figure 56. Simulation results from for the Building 24 positions, with no multipath contribution. Average of 10,000 trials.

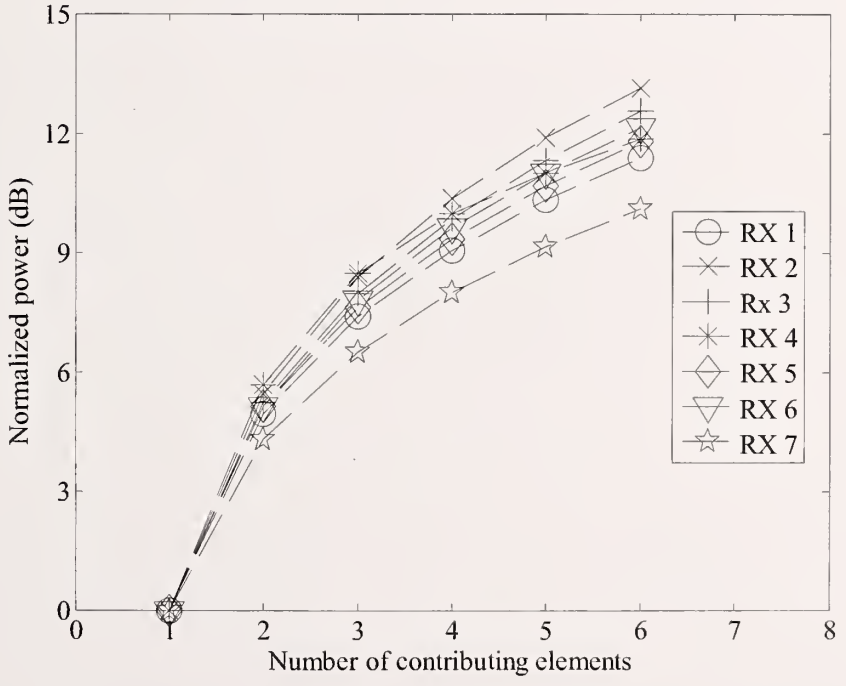

Figure 57. Simulation results for the Building 24 positions, with three multipath components. Average of 10,000 trials.

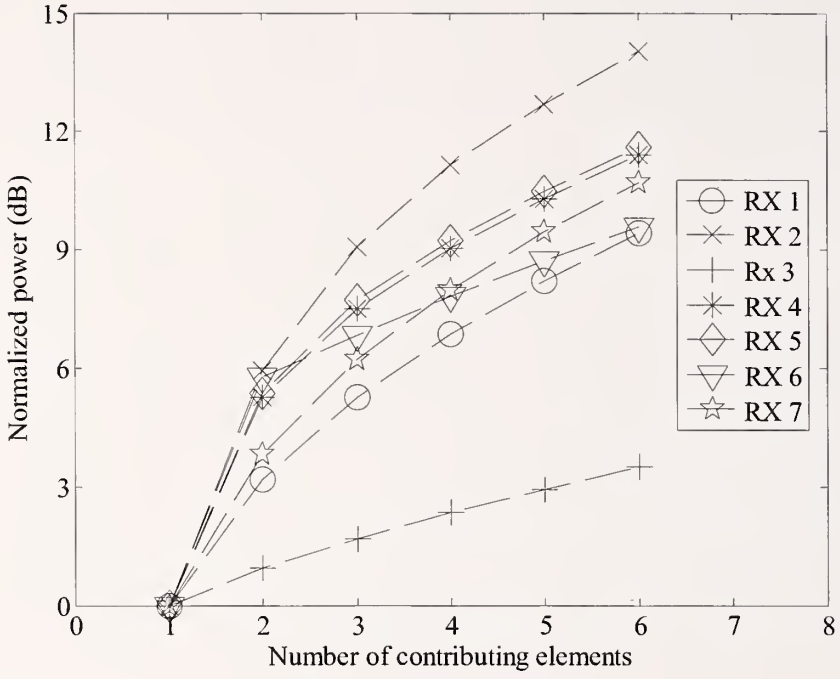

Figure 58. Simulation results from for the Denver site positions, with no multipath contribution. Average of 10,000 trials.

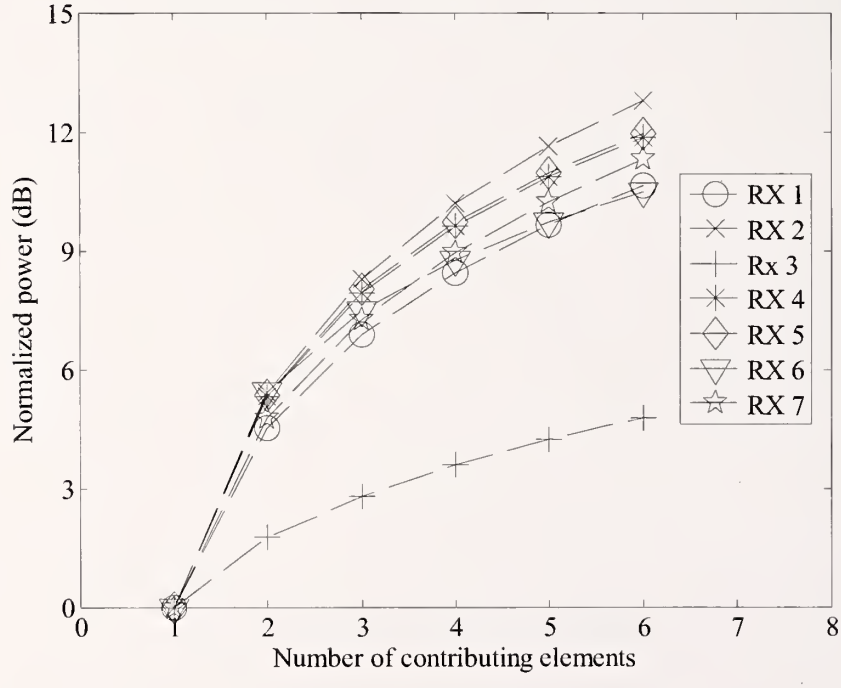

Figure 59. Simulation results from for the Denver site positions, with ten multipath components. Average of 10,000 trials.

NIST Technical Publications

Periodical

Journal of Research of the National Institute of Standards and Technology—Reports NIST research and development in metrology and related fields of physical science, engineering, applied mathematics, statistics, biotechnology, and information technology. Papers cover a broad range of subjects, with major emphasis on measurement methodology and the basic technology underlying standardization. Also included from time to time are survey articles on topics closely related to the Institute's technical and scientific programs. Issued six times a year.

Nonperiodicals

Monographs—Major contributions to the technical literature on various subjects related to the Institute's scientific and technical activities.
Handbooks—Recommended codes of engineering and industrial practice (including safety codes) devel- oped in cooperation with interested industries, professional organizations, and regulatory bodies.
Special Publications—Include proceedings of conferences sponsored by NIST, NIST annual reports, and other special publications appropriate to this grouping such as wall charts, pocket cards, and bibliographies.
National Standard Reference Data Series—Provides quantitative data on the physical and chemical properties of materials, compiled from the world's literature and critically evaluated. Developed under a worldwide program coordinated by NIST under the authority of the National Standard Data Act (Public Law 90-396). NOTE: The Journal of Physical and Chemical Reference Data (JPCRD) is published bimonthly for NIST by the American Institute of Physics (AIP). Subscription orders and renewals are available from AIP, P.O. Box 503284, St. Louis, MO 63150-3284.
Building Science Series—Disseminates technical information developed at the Institute on building materials, components, systems, and whole structures. The series presents research results, test methods, and performance criteria related to the structural and environmental functions and the durability and safety characteristics of building elements and systems.
Technical Notes—Studies or reports which are complete in themselves but restrictive in their treatment of a subject. Analogous to monographs but not so comprehensive in scope or definitive in treatment of the subject area. Often serve as a vehicle for final reports of work performed at NIST under the sponsorship of other government agencies.
Voluntary Product Standards—Developed under procedures published by the Department of Commerce in Part 10, Title 15, of the Code of Federal Regulations. The standards establish nationally recognized requirements for products, and provide all concerned interests with a basis for common understanding of the characteristics of the products. NIST administers this program in support of the efforts of private-sector standardizing organizations.

*Order the **following** NIST publications—FIPS and NISTIRs—from the National Technical Information Service, Springfield, VA 22161.*

Federal Information Processing Standards Publications (FIPS PUB)—Publications in this series collectively constitute the Federal Information Processing Standards Register. The Register serves as the official source of information in the Federal Government regarding standards issued by NIST pursuant to the Federal Property and Administrative Services Act of 1949 as amended, Public Law 89-306 (79 Stat. 1127), and as implemented by Executive Order 11717 (38 FR 12315, dated May 11,1973) and Part 6 of Title 15 CFR (Code of Federal Regulations).
NIST Interagency or Internal Reports (NISTIR)—The series includes interim or final reports on work performed by NIST for outside sponsors (both government and nongovernment). In general, initial distribution is handled by the sponsor; public distribution is handled by sales through the National Technical Information Service, Springfield, VA 22161, in hard copy, electronic media, or microfiche form. NISTIR's may also report results of NIST projects of transitory or limited interest, including those that will be published subsequently in more comprehensive form.

NIST Technical Publications

Periodical

Journal of Research of the National Institute of Standards and Technology—Reports NIST research and development in metrology and related fields of physical science, engineering, applied mathematics, statistics, biotechnology, and information technology. Papers cover a broad range of subjects, with major emphasis on measurement methodology and the basic technology underlying standardization. Also included from time to time are survey articles on topics closely related to the Institute's technical and scientific programs. Issued six times a year.

Nonperiodicals

Monographs—Major contributions to the technical literature on various subjects related to the Institute's scientific and technical activities.
Handbooks—Recommended codes of engineering and industrial practice (including safety codes) devel- oped in cooperation with interested industries, professional organizations, and regulatory bodies.
Special Publications—Include proceedings of conferences sponsored by NIST, NIST annual reports, and other special publications appropriate to this grouping such as wall charts, pocket cards, and bibliographies.
National Standard Reference Data Series—Provides quantitative data on the physical and chemical properties of materials, compiled from the world's literature and critically evaluated. Developed under a worldwide program coordinated by NIST under the authority of the National Standard Data Act (Public Law 90-396). NOTE: The Journal of Physical and Chemical Reference Data (JPCRD) is published bimonthly for NIST by the American Institute of Physics (AIP). Subscription orders and renewals are available from AIP, P.O. Box 503284, St. Louis, MO 63150-3284.
Building Science Series—Disseminates technical information developed at the Institute on building materials, components, systems, and whole structures. The series presents research results, test methods, and performance criteria related to the structural and environmental functions and the durability and safety characteristics of building elements and systems.
Technical Notes—Studies or reports which are complete in themselves but restrictive in their treatment of a subject. Analogous to monographs but not so comprehensive in scope or definitive in treatment of the subject area. Often serve as a vehicle for final reports of work performed at NIST under the sponsorship of other government agencies.
Voluntary Product Standards—Developed under procedures published by the Department of Commerce in Part 10, Title 15, of the Code of Federal Regulations. The standards establish nationally recognized requirements for products, and provide all concerned interests with a basis for common understanding of the characteristics of the products. NIST administers this program in support of the efforts of private-sector standardizing organizations.

*Order the **following** NIST publications—FIPS and NISTIRs—from the National Technical Information Service, Springfield, VA 22161.*

Federal Information Processing Standards Publications (FIPS PUB)—Publications in this series collectively constitute the Federal Information Processing Standards Register. The Register serves as the official source of information in the Federal Government regarding standards issued by NIST pursuant to the Federal Property and Administrative Services Act of 1949 as amended, Public Law 89-306 (79 Stat. 1127), and as implemented by Executive Order 11717 (38 FR 12315, dated May 11,1973) and Part 6 of Title 15 CFR (Code of Federal Regulations).
NIST Interagency or Internal Reports (NISTIR)—The series includes interim or final reports on work performed by NIST for outside sponsors (both government and nongovernment). In general, initial distribution is handled by the sponsor; public distribution is handled by sales through the National Technical Information Service, Springfield, VA 22161, in hard copy, electronic media, or microfiche form. NISTIR's may also report results of NIST projects of transitory or limited interest, including those that will be published subsequently in more comprehensive form.

U.S. Department of Commerce
National Bureau of Standards and Technology
325 Broadway
Boulder, CO 80305-3328

Official Business
Penalty for Private Use $300